Politecnico di Torino
First School of Engineering
Degree Course in Mathematical Engineering

BIDIMENSIONAL TURBULENT TRANSPORT IN THE PRESENCE OF A STABLE STRATIFICATION OR NOT

Supervisor:
Daniela Tordella

Author:
Francesca De Santi

James Riley

Lauris Ducasse

Preface

Fluid and plasma turbulence is ubiquitous in nature, at all scales from coffee cup to universe. Two-dimensional turbulence has the special distinction that it is nowhere realized in nature or the laboratory but only in computer simulations. Its importance is two-fold: first, that it idealizes geophysical phenomena in the atmosphere, oceans and magnetosphere and provides a starting point for modeling these phenomena second, that it presents some special and interesting phenomena.

For these reasons we decided to perform two numerical experiments on flat turbulence. The first is the analysis of a energy transport and will lead us to estimate the main differences between the bi- and three-dimensional case. We also want to analyze the intermittency of these motions and try to estimate the time take to loose the memory of the initial condition.
Secondly, we considered the vorticity field as a vertical section of an atmospheric and/or oceanic flow. We then added the effect of stratification on mixing and attempted to conduct the same type of analysis, achieving results very interesting.

This text is organized as follows. The next chapter summarizes the findings and the main features of classical turbulence. In the second chapter, two-dimensional turbulence is introduced with its main phenomena, such as the inverse cascade of energy. Chapter 3 instead presents the first numerical experiment and the results obtained from it.
The fourth chapter introduces the second part of the study and summarizes the theoretical aspects related to the stratified flows. The numerical experiment on them is described and analyzed in Chapter 5. Finally, in the last chapter are collected the main results obtained in this study.

The entire study was conducted in collaboration with James Riley and Oscar Flores of the University of Washington (Seattle). I take this opportunity to thank them for their help and suggestions they have given me. I also thanks Jost von Hardemberg (ISAC CNR) for giving me the opportunity to use and modify the code he wrote

Contents

Chapter 1

Introduction to turbulence

Turbulence is a omnipresent phenomenon of Nature. In our everyday life, we either rarely notice it when swimming, driving a car, riding a bike, skating, or suddenly pay serious attention to it, when the ride gets bumpy on board a plane on stormy weather or when flying over tall mountains.
Actually, the diversity of situations where we discover turbulence as an important scientific phenomenon is impressive: flow around ships and aircrafts, combustion in car engines and plane turbines, flow in the ocean, atmosphere, air flow in lungs, flow of blood in arteries and heart, flow in pipelines, even the dynamics of the financial markets can also be viewed as analogous to turbulent flows.
The entire Universe appears to be in a state of turbulent motion, and turbulence seems to be a decisive factor helping in the formation of stars and solar systems, as indicated by astronomical observations and theoretical considerations in astrophysics.
From the large variety of situations mentioned above, many of them are cases in which turbulence is attractive from the point of view of the engineer, since studying it leads to technological improvement. It is more fruitful then to model regions where the turbulent flows interact with boundaries, and then learn how to control and apply them.
For the physicist, the interesting part is how the small-scale structure of turbulence is organized, preferably isolated from any boundary effects. This is where universal aspects can be sought, in the sense that they should be independent of the nature of the fluid or the geometry of the problem. It is universality that makes turbulence an exciting research subject for physicists and mathematicians.

Skipping over the dictionary definition, which does not suffice to characterize the modern physical sense of the word, we stop at the definition given in 1937 by Taylor and Von Karman: "*Turbulence is an irregular mo-*

tion which in general makes its appearance in fluids, gaseous or liquid, when they flow past solid surfaces or even when neighboring streams of the same fluid past or over one another".
To make this more clear, we need to use the terminology of fluid dynamics. Flows of gases and liquids can be divided into two very different types: "laminar" flows, which are smooth and regular, and "turbulent", totally opposite, in which physical quantities as velocity, temperature, pressure, etc. fluctuate in a sharp and irregular manner in space and time, the latter being actually the more natural state of a flow.

In the following section will discuss briefly the history of turbulence from Leonardo to Kolmogorov. In the second section we will provide a brief overview of the motion equation. Finally in the last section we will talk about the statistical description of turbulence, particularly concerning the phenomenon of intermittency.

1.1 History of turbulence

It appears that Leonardo Da Vinci was probably the first to distinguish this special state of the fluid motion and use the term "turbulence".
Modern turbulence started with the experiments of Osborne Reynolds in 1883, who analyzed the conditions under which laminar flows of fluids in pipes become turbulent. The study led to a criterion of dynamical stability based on the "Reynolds number":

$$Re = \frac{\rho U L}{\mu} = \frac{U L}{\nu} \tag{1.1}$$

where U and L are the characteristic velocity and length scales of the flow and ν is the kinematic viscosity.
The Reynolds number may be interpreted as the ratio of inertial to viscous forces present in the fluid, and for an incompressible flow, it is the only control parameter of that system.
Intuitively, as Frisch points out in his book on turbulence [3], its value can also be seen as an indicator for the degree of symmetry of the flow. This can easily be imagined in the experimental situation of a flow past a cylinder. For values of the Reynolds number departing from 1, visualizations of the flow show a gradual increase of the degree of asymmetry in the flow surrounding the obstacle, before and after it.
Based on the technological interest raised by the remarkable momentum transfer properties of the large scales of turbulence, experiments in the beginning of the 20th century led to decisive advances in the theory of turbulence.

Representative of this time are the so-called semi-empirical approaches made by great fluid-dynamicists, such as G. Taylor, L. Prandtl and T. Von Kármán in the 1920s and '30s, which were used to solve important practical problems. In a remarkable paper, Lewis Fry Richardson advanced in 1922 the assumption that turbulence is organized as an hierarchy of eddies of various scales, each generation borrowing energy from its immediately larger neighbor in a "cascade" process of eddy-breakdown [11]. This picture, though more appropriate in wavenumber space, was poetically immortalized in his book inspired from observation of clouds and the verses of Jonathan Swift: *"Big whorls have little whorls, which feed on their velocity; and little whorls have lesser whorls, and so on to viscosity (in the molecular sense)"*
This era culminated with the now fundamental ideas of Andrei Nikolaevich Kolmogorov in the "theory of locally isotropic turbulence" (1941) [7]. Inspired by Richardson's energy cascade description, he assumed that with each step in the energy transfer towards smaller scales, the anisotropic influence of the large scales will gradually be lost, such that at sufficiently small scales the flow will be statistically homogeneous and isotropic. This steady situation, characterized by a mean flux of energy $\langle e \rangle$, was postulated by Kolmogorov to be universal and determined by only one parameter, $\langle e \rangle$. Moving further down the scales, there comes a length-scale where the flow gradients are so large that viscous effects can no longer be ignored. The scale is determined (in a dimensional argument) from the viscosity ν and $\langle e \rangle$:

$$\eta = \left(\frac{\nu^3}{\langle e \rangle} \right)^{1/4} \tag{1.2}$$

We introduce below the famous self-similarity hypotheses in their original form (according to Hinze [5]):

- (a)At sufficiently large Reynolds numbers there is a range of high wavenumbersv(inertial-range) where the turbulence is statistically in equilibrium and uniquely determined by the parameters $\langle e \rangle$ and ν. This state of equilibrium is universal.

- (b)If the Reynolds number is infinitely large, the energy spectrum in the inertial range is independent of ν and solely determined by the parameter $\langle e \rangle$.

1.2 The nature of the turbulence

The equations that govern turbulence are essentially a form of Newton's law for the motion of a fluid that is forced, at large scales, and affected by viscous dissipation, at small-scales:

$$\rho\frac{D\mathbf{u}}{Dt} = \rho\frac{\partial\mathbf{u}}{\partial t} + \rho\mathbf{u}\cdot\nabla\mathbf{u} = -\nabla p + \mu\Delta\mathbf{u} + \mathbf{F} \tag{1.3}$$

Here the vector $\mathbf{u} = \mathbf{u}(\mathbf{x}, t)$ denotes the velocity field at position $\mathbf{x}$ at moment t, $p = p(\mathbf{x}, t)$ the pressure, $\mathbf{F}$=$\mathbf{F}$($\mathbf{x}$, t) the forcing, ρ is the density and μ is the kinematic viscosity.
This equation is known as the Navier-Stokes equation (N-SE), after the physicists who added the viscous term $\mu\Delta\mathbf{u}$, C.L.M.H. Navier in 1827 and G.G.Stokes in 1845. Through this term, the kinetic energy is no longer conserved, but lost to heat.
The Navier-Stokes equation is a continuum equation.
Later on we will learn that in three-dimensional turbulence fluid motion occurs on smaller and smaller scales if the Reynolds number increases. Still, it can be proven that these scales will never be so small that the scale of molecular graininess of of the fluid is reached. Remarkably, the argument proving this rests intimately on the Kolmogorov scaling hypotheses of turbulence. The flow velocities we consider are much smaller than the velocity of sound, which gives the incompressibility condition:

$$\nabla\cdot\mathbf{u} = 0 \tag{1.4}$$

Given an initial state of the flow field, together with the prescription of the velocity at the boundaries, the N-SE suggests that the evolving field $\mathbf{u}(\mathbf{x}, t > 0)$ is deterministic. However, we are uncertain about the uniqueness of the solution and therefore cannot characterize the phenomenon of turbulence as deterministic chaos. Moreover, the number of degrees of freedom of a turbulent flow is extremely large, which warrants a statistical rather than a deterministic description.
Furthermore, we can bring the complexity of turbulence in three main:

- Nonlinearity - the term $u_j\dfrac{\partial u_i}{\partial x_j}$ in the N-SE
- Existence and smoothness of solutions at all time
- Non-locality - to determine the local fields one has to integrate over the entire space.

A more rewarding approach to deal with the extreme complexity of turbulence is a statistical description.

1.3 Statistical approach and phenomenology

In principle, the phenomenology of turbulence is characterized by simple statistical quantities, such as averages, probability distribution functions, spectra, correlations, etc., which are calculated from data experimentally measured or from direct computer simulations. In general, the term "averaging" is never equivalent to a proper ensemble average (over all possible states of the system), but ergodicity is invoked to replace it by time-averaging or mixed time and limited spatial averaging. These tools are sufficient to reveal some of the most important universal features of turbulence.

1.3.1 Small-scales of turbulence and universality

While turbulence at large Reynolds numbers consists of a wide range of dynamical scales that contain its energy, they are bounded naturally by a largest scale at which turbulence is stirred, and a smallest scale η, defined in 1.2, where most of the energy is dissipated. By small scales we will understand the dissipative range close to η and the inertial range postulated by the first Kolmogorov hypothesis (a). Phenomenological studies of turbulence are mostly aimed at the study of the small scales, since it is here that universal properties of turbulence are seen, and their characterization is considered important for the "turbulence problem".
The second hypothesis of Kolmogorov (b) implies that small-scale turbulence is isotropic and homogeneous at sufficiently large Reynolds numbers, and its statistics will be determined only by the average dissipation rate

$$\langle e \rangle = \frac{\nu}{2} \left\langle \left(\frac{\partial u_i}{\partial x_j} + \frac{\partial u_j}{\partial x_i} \right)^2 \right\rangle \tag{1.5}$$

where ν is the flow viscosity. If we consider the histogram of the fluctuations of normalized velocity increments over a small-scale separation $\Delta\mathbf{u}(\mathbf{x})/(\mathbf{x}\,\langle e \rangle)^{1/3}$, it follows then from (b) that this statistical quantity should be universal, i.e. independent of the flow, Reynolds number or $\mathbf{x}$. We will see next how the Kolmogorov prediction is reflected and can be quantized using simple statistical tools.

1.3.2 Structure function and intermittency

One of the most common statistical quantities used in the phenomenology of turbulence is the *structure function*. We define the structure function of

order p to be

$$\mathcal{S}_p(\mathbf{r}) = \langle \Delta\mathbf{u}(\mathbf{x})^p \rangle = \int_{-\infty}^{+\infty} \mathcal{P}(\Delta(\mathbf{u}))\Delta(\mathbf{u})^p d(\Delta\mathbf{u}) \tag{1.6}$$

where $\Delta\mathbf{u}$ are the velocity increments and $\mathcal{P}(\Delta u)$ is their probability distibution function. The postulated universality of the normalized $\mathcal{P}\Delta u/(x\,\langle e \rangle)^{1/3}$ implies that structure functions exhibit scaling behavior for high Reynolds numbers

$$\mathcal{S}_p(x) = C_p(x\,\langle e \rangle)^{p/3} \tag{1.7}$$

when the separations $\mathbf{x}$ are within the inertial range, with C_p universal constants.
The values of the scaling exponents $\zeta_p = p/3$ follow from the postulate.
The equivalent form of the above relation for order $p = 2$ gives the well-known scaling law for the energy spectrum

$$E(k) = C\,\langle e \rangle^{2/3}\,k^{-5/3} \tag{1.8}$$

The only known exact relation for structure functions can be derived directly from the Navier-Stokes equations, namely the *Kolmogorov 4/5 law*

$$\mathcal{S}_3^L(\mathbf{x}) = -\frac{4}{5}\langle e \rangle\,\mathbf{x} \tag{1.9}$$

For high orders $p \geq 4$, it is well-known the that scaling exponents ζ_p deviate from the Kolmogorov dimensional prediction, that is $\zeta_p < p/3$. These deviations are known as anomalous scaling and imply that the form of the probability distributions $\mathcal{P}(\Delta(\mathbf{u})$ will vary inside the inertial range, such that with the decrease of the scale towards the dissipative range, their 'tails' will be increasingly flared out.
This phenomenon is called *intermittency* and the anomalous scaling is a measure of it, since higher orders emphasize increasingly larger velocity excursions $\Delta\mathbf{u}(\mathbf{x})$.
To account for intermittency, the refined (RSH) versions of the self-similarity hypotheses were proposed by Kolmogorov (1962) [8], which incorporated the suggestion of Obukov that the mean energy dissipation rate exhibits strongly non-Gaussian fluctuations. In the case of anomalous scaling, one defines a local mean dissipation rate

$$e_x(\mathbf{x}, t) = \int_{V_r} e dV \tag{1.10}$$

such that its own scaling exponent

$$\langle e_r \rangle^p \approx r^{\tau_p} \tag{1.11}$$

will contribute to the new scaling

$$\langle \Delta \mathbf{u}^p(\mathbf{x}) \rangle = C'_p (\langle e_x \rangle \mathbf{x})^{p/3} \tag{1.12}$$

which exponents

$$\zeta_p = p/3 + \tau_p \tag{1.13}$$

Implicitly, the constants C'_p lose their universality (the famous "Landau objection", originally formulated in 1944 [10]). The failure of the Kolmogorov theory to explain the anomalous scaling does not stop here however. Continuous improvement of experiments on intermittency brings increasing evidence that a description of turbulence beyond the Kolmogorov formulation, which dominated the turbulent research for more than half a century, is acutely needed.
A number of intermittency models were proposed, which attempt to explain in particular the anomalous scaling exponents. The most popular model to explain the anomalous scaling exponents is the multifractal model of Frisch (1985[4]).

Chapter 2

Two-Dimensional Turbulence

Probably the most common statement made about two-dimensional turbulence is that it does not exist. While factually correct, it rather misses the point. There are many flows whose large scale behavior is, in some sense, two dimensional. Large-scale atmospheric and oceanic flows fall into this category, if only because of the thinness of the atmosphere and oceans in comparison with their lateral dimensions. Moreover, both rapid rotation and strong stratification tend to promote two-dimensional flows through the propagation of internal waves, and, of course, strong magnetic fields promote two-dimensionality. While no flow will ever been truly two-dimensional, it seems worthwhile to examine the dynamics of strictly two-dimensional motion in the hope that it sheds light on certain aspects of real, 'almost' two-dimensional phenomena.

In moving from three- to two-dimensions we greatly simplify the equations. Most importantly, we throw out vortex stretching. One might expect, therefore, that two-dimensional turbulence should be much simpler than isotropic turbulence. Mathematically, this is correct, as it must be. Curiously though, the physical characteristics of two dimensional turbulence are, in many ways, more counter-intuitive than conventional turbulence. At least, this is the case for one brought up in the traditions of Richardson and Kolmogorov. For example, in two dimensions, there is an *inverse cascade* of energy, from the small to the large, as small vortices merge to from larger one.

In the next section we will see the major differences between two- and three-dimensional turbulence. In the second one we will give a phenomenological description of the evolution of two-dimensional turbulence. In the last section we will mention the main results obtained so far on the energy spectrum and will explain the inverse cascade phenomenon in a more rigorous way.

2.1 First comparison between two- and three-dimensional turbulence

There is in general agreement that all the flow proprieties of Newtonian fluids in two (2D) or three (3D) dimensions are encompassed in the N-SE for the velocity (equation 1.3), if we assumed that the flow is incompressible. The different between 2D and 3D flows is not apparent from this equation but becomes so on taking its curl to obtain an equation for the vorticity $\omega = \nabla \times \mathbf{u}$ in an incompressible framework. For each component, i, of ω and $\mathbf{u}$

$$\frac{D\omega_i}{Dt} = (\omega \cdot \nabla)\mathbf{u_i} + \nu \mathbf{\Delta} \omega_\mathbf{i} \tag{2.1}$$

Consider the special case where, at a certain instant of time, $\omega = (\mathbf{0}, \mathbf{0}, \omega_\mathbf{z})$, with the viscous damping term being small. Then

$$\frac{D\omega_z}{Dt} = \omega_z \frac{\partial u_z}{\partial z}$$

If $\partial u_z / \partial z > 0$, ω_z will momentarily commence growing at an exponential rate. Clearly the vorticity is not a conserved quantity in 3D; it can magnified by appropriately oriented velocity gradient. As an example, imagine water circulating as it flows downward trough a funnel. By conservation of the angular momentum, the flow will pick up angular speed as it proceeds downward trough the concentration, so that the magnitude of the vorticity is increased in the direction of the velocity gradient. This amplification effect is called *vortex stretching*.

Vortex stretching is at the core of the description of the turbulence energy cascade from the large scales to small scales in turbulence. In general, in turbulence fluid elements are more lengthened than squeezed, on average. In the end, this results in more vortex stretching than vortex squeezing. For incompressible flow, due to volume conservation of the fluid elements, the lengthening implies thinning of the fluid elements in the directions perpendicular to the stretching directions. this reduce the radial length scale of the associated vorticity. Finally, at the scales of the order of the Kolmogorov micro scales, the turbulence kinetic energy is dissipated into heat through the action of the molecular viscosity.

Also in this simplified framework, it highlights another fundamental property of the vorticity dynamics in 3D.
We hypothesized that for a given instant vorticity exists only in one direction, ie $\omega_x = \omega_y = 0$ and $\omega_z \neq 0$. Since we are considering a three-dimensional flow,

generally may exist $\partial u_x/\partial z$ and $\partial u_y/\partial z$ nonzero. By the vorticity equation we have

$$\frac{D\omega_x}{Dt} = \omega_z \frac{\partial u_x}{\partial z} \qquad \frac{D\omega_y}{Dt} = \omega_z \frac{\partial u_y}{\partial z}$$

This means that in the instant immediately following this one, there is nonzero component of velocity in all directions. This phenomenon is called the *spontaneous three-dimensionalization of the field.*

In three dimensional turbulence vortex stretching and the spontaneous three-dimensionalization of the field are two important dynamical effects, which causes the emergence of filamentary vortex tube, as those shown in figure 2.1. These vortices seems to be the dominant flow structures in fully developed, homogeneous and isotropic turbulence.

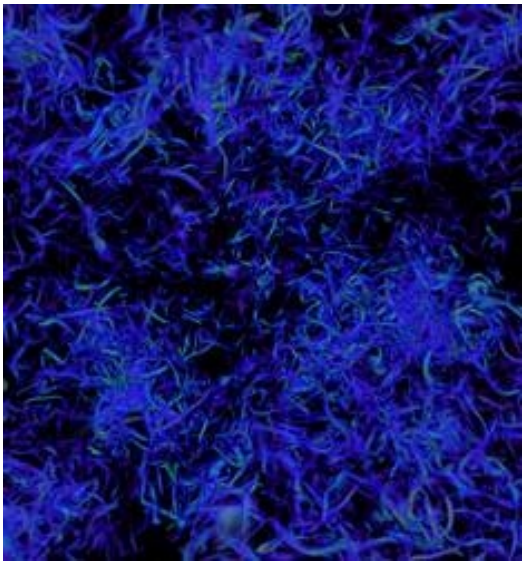

Figure 2.1: An example of three dimensional turbulence

This phenomenas are absent in two dimensions, because the velocity gradient is always perpendicular to the vorticity, which is necessarily perpendicular to the plane of the motion. Hence the first term on the right in equation 2.1 is absent, assuring that for an inviscid flow if forcing is absent, we have

$$\frac{D\omega}{Dt} = 0$$

Of course, $\omega(\mathbf{x}, \mathbf{t})$ can change locally, but it mean value averaged over a sample area A

$$Z = \frac{1}{A}\int_A \omega^2 d^2 r$$

is a constant of the motion, as are all other vorticity moments. This quantity is called the *enstrophy*.
In other words, in two dimensional turbulence there is an additional important constant of motion: the enstrophy. The enstrophy constant leads to equilibrium in which a large fraction of the energy is condensed into the largest spatial scales of motion.
In conclusion, what distinguishes it most from 3D turbulence is the conservation of vorticity along fluid particle path when viscosity and forcing are ignored. As a consequence enstrophy cannot increase under the sole action of non linearity.

2.2 Vortex interaction

The phenomenology of turbulence, in three or two dimensions, is usually phrased in therms of *eddies*. An eddy itself is not a well defined object, thought there have been many recent attempts using wavelet to better define the concept.
Loosely speaking it is a region in a fluid that is behaving coherently. The extent of an eddy is dictated by boundaries within which an arbitrary determination is made some sort of structure exist. Thus an eddy can be a single large region of rotation, such as the whirlpool which forms above a bathroom drain. Or an eddy can be a large region containing many smaller eddies which are interacting with one another while behaving distinctly (again by an arbitrary determination) from other neighboring cluster of eddies.
Two important properties that are associated with an eddy are size and energy. These two properties allow predictions about energy motion in fluids to be made if some knowledge of how eddies interact in the system is known.

In 2D flows, one way in which eddies (which assume the more familiar label "vortices") interact which each other is through a process known as *vortex cannibalization*. A cannibalization event is when two neighboring eddies of like rotational sense merge to form a single larger eddy. When cannibalization occurs energy flows out to the length scales of the initial eddies and into the length scale of the final eddy. "*When a number of vortices having the same sense of rotation exist in proximity to one another, they tend to approach one another, and to amalgamate into intense vortex*"(Aryton, 1919).

In a 2D turbulent flow, many eddies are generally created at a small length scale called the energy injection scale, r_{inj}. The expectation is that through interaction by cannibalization these small eddies cluster and merge into larger eddies. These larger eddies are also expected to cluster and merge to form

even larger eddies and so on. This means that energy, initially injected into the turbulence at the length scales r_{inj} should gradually be moved by consecutive cannibalization events to larger length scales. In figure 2.2 we show the scheme of the eddy cannibalization.

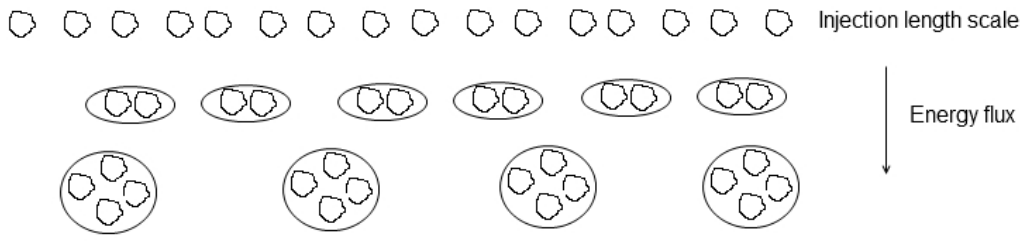

Figure 2.2: The scheme of the eddy cannibalization in 2D turbulence

This type of energy motion constitutes an inverse energy cascade. Presumably each eddy is itself formed by the clustering of smaller eddies, which in run in turn are formed by even smaller eddies. As long as the eddies at the very smallest scale, the injection scale, are being continuously created to replenish those which are cannibalized, the inverse cascade range is scale-invariant. That is to say that no length scale in the inverse cascade range can be distinguished from any other length scale that is also in the range. Scale invariance is exceedingly important from a theoretical stand point. The assumption of scale invariance of fields, such as the probability of velocity difference on a length scale r, allow important prediction about turbulent to be made.

Before discussing locality, a delicate point must be made. if the eddies at the injection length scale are not being continuously replenished then the number of eddies at the smallest scales gradually begins to decrease as more and more eddies are lost to cannibalization events. To maintain an inverse cascade range, then, the turbulence has to be continuously forced. That is, eddies must be continuously created at the energy injection scale. If the turbulence is not forced then the cascade range will eventually consume itself from small scale up, ultimately leading to a state which describes as a diffuse gas of large individual eddies (eddies not made of clusters of smaller eddies). The term *coarsening* is used to describe decaying 2D turbulence behavior in order to distinguish it from the inverse energy cascade.

The second property assumed to hold in the inverse cascade is locality of interaction. This property refers to constraints on the manner i which eddies interact. If an eddy of very small size is close to, or embedded in, an eddy of exceedingly large size, the small eddy will merely be swept along

by the large and not strongly deformed. Likewise the large eddy will be not significantly effected by it's small companion. Since neither of the eddies is strongly deformed, the cannibalization process is expected to happen over a long period of time. On the other hand, two neighboring eddies of similar size interact and deform one another strongly, and thus the cannibalization process happens swiftly. Energy transfer by cannibalization is therefore most efficient when occurring between similarly size length scales, this is what meant by locality. Due to locality, the kinetic energy at small scales in the inverse cascade is expected to be moved to large scales in a continuous manner, stepping through the intervening length scales by local interactions rather than making large lenght scale jumps by the merger of a small and large eddy. Hence the term *cascade*.

The picture of 2D turbulence and it's inverse cascade is now almost complete. Energy is continually injected into a flow in the form of small eddies. These small eddies cluster to form large eddies moving energy to larger scales. In turn the eddy clusters themselves cluster to form larger clusters of eddy clusters, etcetera. In this etcetera that is the concern. At what point does the vortex merger process and growth of larger and larger eddies stop? That is, how is the energy injected into a 2D turbulent thermostated?
Consider first the thermostating mechanism in 3D turbulence. In 3D turbulence there exists a direct energy cascade: energy is moved from large to small scales by eddy stretching. Eventually, through continuous vortex stretching, a smallest eddy scale is reached, at which point the kinetic energy contained in these small eddies is dissipated into heat by the fluids internal viscosity. all of the energy that in injected into the large length scales of a 3D turbulent flow is eventually exhausted by viscosity at the small length scale.

Internal viscosity is a short range force, only becoming a good thermostat when the kinetic energy reaches small length scales. Thermostating in not a issue in 3D where the direct cascade takes energy down to such small scales. In 2D, however, the inverse cascade moves energy in the flow would continue to build up as larger and larger eddies form. What is needed to maintain 2D forced turbulence in a steady state and stop the inverse cascade process in some sort of external dissipation mechanism which is an effective thermostat at large length scales. In other words, some sort of dissipation mechanism that is not internal to the fluid itself must exist to take energy out of large length scales and dictate the largest size eddies that can be formed by the cascade.

Fortunately, 2D experiments are almost always coupled to the surrounding 3D environment by frictional forces. In these experiments this external frictional force provide the turbulence with an effective large scale thermostat and sets the largest length scales which can be reached by the inverse

cascade process. The inclusion of an external thermostat completes this phenomenological description of the inverse energy cascade.
Figure 2.3 shows an example of two dimensional turbulence in which we can abserve the processes just discussed.

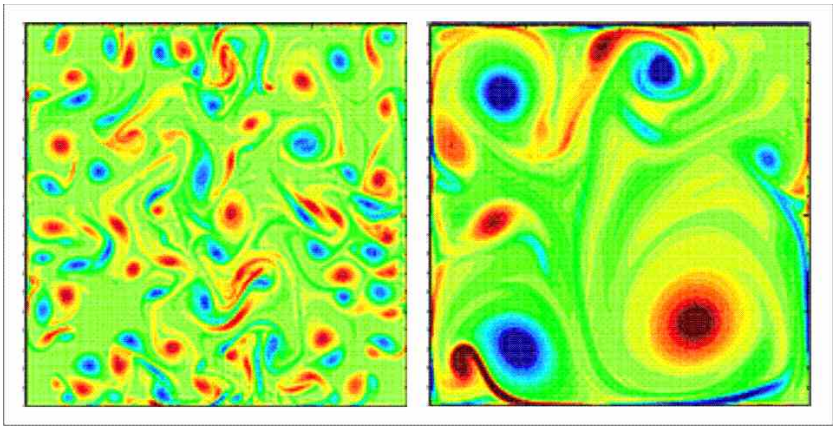

Figure 2.3: Time evolution of a two dimensional turbulence that shows the cannibalization process

2.3 Batcherol's self similar spectrum and the inverse energy cascade

We shall restrict ourself to strictly two-dimensional turbulence, $\mathbf{u} = (\mathbf{u_x}, \mathbf{u_y}, \mathbf{0})$ and $\omega = (\mathbf{0}, \mathbf{0}, \omega)$, and to turbulence which is homogeneous ans isotropic. We shall ignore all body force, and address the problem of freely evolving turbulence.
We define the characteristic velocity u though $u^2 = \langle u_x^2 \rangle = \left\langle u_y^2 \right\rangle$. All existing phenomenological theories are based on the two equations

$$\frac{d}{dt}\left[\frac{1}{2}\left\langle u^2 \right\rangle\right] = -\nu \left\langle \omega^2 \right\rangle \tag{2.2}$$

$$\frac{d}{dt}\left[\frac{1}{2}\left\langle \omega^2 \right\rangle\right] = -\nu \left\langle (\nabla\omega)^2 \right\rangle \tag{2.3}$$

This state that the kinetic energy density, $1/2\,\langle u^2 \rangle$, and the enstrophy, $\langle \omega^2 \rangle$, both decline monotonically in freely evolving two-dimensional turbulence. The first of these relationships comes from taking the product of $\mathbf{u}$ with

$$\frac{D\mathbf{u}}{Dt} = -\frac{1}{\rho}\nabla p - \nu \nabla \times \omega$$

which yields

$$\frac{D}{Dt}\left[\frac{\mathbf{u^2}}{2}\right] = -\nabla \cdot \left[\frac{p\mathbf{u}}{\rho}\right] - \nu\left[\omega^2 - \nabla \cdot (\mathbf{u})\right]$$

We now average this equation, nothing that an ensemble average is equivalent to a spatial average (for the ergodic theorem, see Halmos 1956), and the statistical homogeneity of the turbulence ensures that all divergences integrate to zero. The end result is 2.2. Similarly, starting with

$$\frac{D\omega}{Dt} = \nu\Delta\omega$$

from which

$$\frac{D}{Dt}\left(\frac{\omega^2}{2}\right) = -\nu\left[(\nabla\omega)^2 - \nabla\left(\omega\nabla\omega\right)\right]$$

we obtain, on forming a spatial average, 2.3.
Now the key point about this two relationship is that, as $Re \to \infty$, u^2 is conserved, since the enstrophy remain finite and bounded by its initial value. This is in stark contrast to three dimensional turbulence, where a decline in ν in accompanied by a rise in $\langle\omega^2\rangle$ in such a way that the dissipation of kinetic energy remains finite (of order u^3/l) as $Re \to \infty$. This conservation of energy in 2D turbulence implies a long-lived evolution for these flows.

In the limit $Re \to \infty$ diffusion becomes small, except at the smaller scales, and so the isovortical lines become material lines, and are continually teased out as the flow evolves so that the vorticity field rapidly adopts the structure of thin, sinuous sheets, like cream stirred into coffee. This filamentation of vorticity feeds an enstrophy cascade, lumps of vorticity are teased out of smaller and smaller scales, which is halted at small enough for viscosity to act, destroying the enstrophy and diffusing the vorticity. As in three dimensions, viscosity plays a passive role, mopping up the enstrophy which has cascaded down from above. The dynamics are controlled by the large scales, and even as $\nu \to \infty$ the destruction of enstrophy remain finite.

This passive role of viscosity led G. K. Batchelor to propose a self similar distribution of energy for the large and intermediate scales. In terms of velocity increments Δu, which represent the r.m.s (root mean square) difference in velocity between two points separated by a distance r, this self-similar energy spectrum takes the form

$$[\Delta u(r)]^2 = u^2 g\left(\frac{r}{ut}\right) \tag{2.4}$$

The argument behind 2.4 is essentially a dimensional one. If the turbulence has evolved long enough for the influence of the initial conditions to be erased,

and viscosity controls only the smallest scales, then all that the large scale remember is u. It follows that u, r and t are the only parameters determining $\Delta u(r)$, and 2.4 is then inevitable. In this model then the integral scale grows as $l \approx ut$. That is, if we divide δu by u and r by $l = ut$, we obtain a self similar energy spectrum valid throughout the evolution of the flow, as is shown in figure 2.4, and so the size of the most energetic eddies must grow as ut.

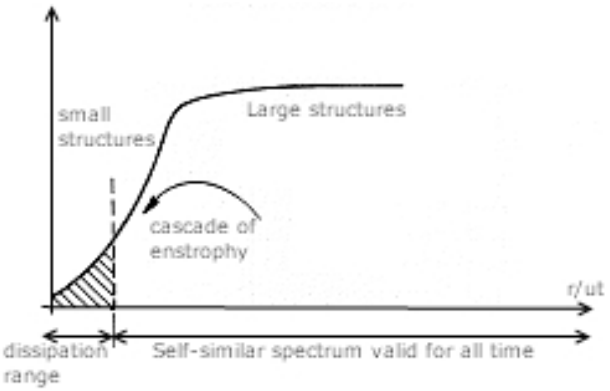

Figure 2.4: Batchelor's universal energy spectrum

For almost thirty years, dating from its introduction in 1969, Batchelor's self-similar energy spectrum, and associated theories by Kraichnan, dominated the literature on two-dimensional turbulence. Note, that this dimensional argument hinges on the flow remembering nothing other than u. It might, for example, also remember the angular momentum square average.

2.3.1 The energy spectrum

For phenomenological considerations made so far, we can assume that the energy is injected through a narrow energy band around the wave number k_{inj}, one can anticipate that the energy transfer to smaller $k(< k_{inj}$ and the enstrophy transfers to larger $k(> k_{inj}$- The energy and enstrophy injection rates are denoted as $\epsilon_t = (\Delta u(l))^3/l$ and $\chi_t = (\Delta u(l))^3/l^3$, respectively. If k_{dis} is the maximum wave number where the viscosity cannot be ignored, the energy and the enstrophy are independent of k in the inertial range $k_{inj} < k < k_{dis}$, that is,

$$\epsilon_t(k) = \epsilon_t(k_{dis}) \qquad \chi_t(k) = \chi_t(k_{dis})$$

By dimensional analysis, one can obtain the relation,

$$k_{dis}^2 \epsilon_t(k_{diss}) \approx \chi_t(k_{diss})$$

Therefore, if $\nu \to 0$ or $k_{diss} \to \infty$, $\epsilon_t(k_{diss}) \to 0$ because $\chi_t(k_{diss})$ is constant over the inertial range. This shows that that the energy cannot be transfered into small scales in the inertial range so that only the enstrophy transfers to small scales. The energy spectrum in the enstrophy cascade regime is obtained by dimensional analysis

$$E(k) \approx \chi_t^{2/3} k^{-3}$$

Similarly, the energy spectrum in the inverse energy cascade can be obtained by showing that only the energy transfers to large scales. It is determined by ϵ_t and k:

$$E(k) \approx \epsilon_t^{2/3} k^{-5/3}$$

Figure 2.5 shows a simple diagram of the energy cascade $E(k)$ in 2D turbulence. When the energy E and the enstrophy Z are injected in k_{inj}, E transfers to small k and ceases at k_{out}, which is the minimum wave number where the energy dissipation cannot be ignored, while Z goes to large k and stops at k_{dis}.

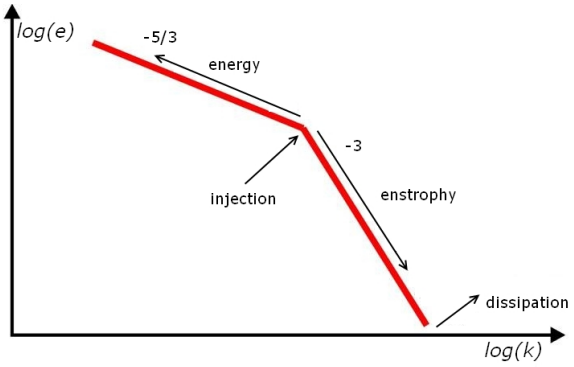

Figure 2.5: Energy spectrum in 2D turbulence

The energy spectrum for 2D turbulence was first calculated by Kraichnan based on statistical physics. However, direct numerical simulations do not very strongly support the k^{-3} law.
In forced turbulence, Legras, Santangelo and Benzi (1988) obtained considerably steeper spectra at small scales, but Borue (1994), using higher Reynolds numbers, obtained reasonably clean k^{-3} spectra. Unfortunately, most of these calculations do not integrate the N-SE, but a modified equation with a high power of the Laplacian as dissipation therm.
The Batchelor-Kraichnan theory also predict a k^{-3} spectrum for decaying turbulence. Again, the numerical evidence is not so strong. Brachet,

Meneguzzi, Politano and Sulem (1998) obtained a k^{-3} spectrum in a moderately long but genuine Navier Stokes simulation. Santangelo, Benzi and Legras (1989) found that, eventually, the energy spectrum becomes quite steep and does so in fashion which depends on the initial conditions. They ascribe this to the formation of hierarchy coherent vortices.

Before concluding this section, we give another physical interpretation of the results just discussed.
In the Batchelor-Kraichnan picture we have two cascades, a direct cascade of enstrophy and an inverse cascade of energy, as anticipated by Aryton in 1919, as more and more energy moves to larger scales, the total energy being conserved. Physically, we can picture this in therm of the filamentation of vorticity, as shown in figure 2.6

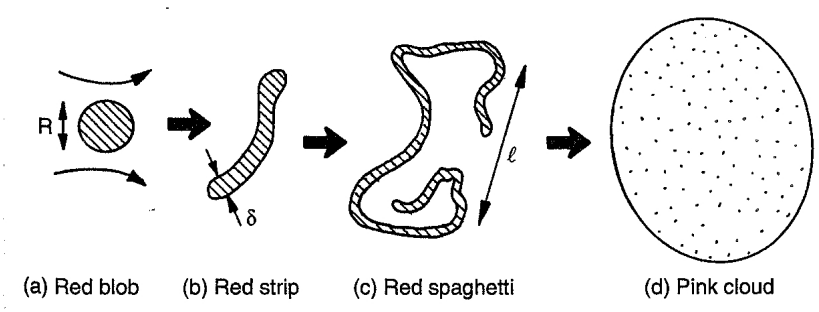

Figure 2.6: Destruction of a lump of vorticity in two dimensional turbulence

A blob of vorticity will be teased out in a strip of thickness δ by eddies whose dimensions are comparable with the blob size, R. Area is conserved by the vortex patch and so δ falls as the characteristic integral dimension, l, increases. The strip is then further teased and twisted by the flow, and in the process l continues to grow at the rate $l \approx ut$ while δ declines. The process ceases, for this particular vortex patch, when δ becomes so small that diffusion sets in, and the red spaghetti becomes the pink cloud.
The direct cascade of enstrophy is associated with the reduction in δ, while the inverse cascade of energy is associated with the grow of l, which characterizes the eddy size associated with the vortex patch.

Chapter 3

Numerical experiment A

The interaction of two isotropic two dimensional turbulent fields of equal integrate scale but different kinetic energy generates the simplest kind of inhomogeneous turbulent field.
The numerical experiment presented in this work consist of two time decaying isotropic fields of kinetic energies E_1 and E_2 initially match over a narrow region. Within this region the kinetic energy varies as a hyperbolic tangent. The following temporal evolution produces a shearless mixing.

The idea of dealing with this study is suggested by an analyses performed by Tordella and Iovieno that simulated a three dimensional mixing [15]. Drawing inspiration from this study, we decided to perform a similar simulation in two dimensional case. The possible applications for this research would be in bettering the predictions of geophysical flow models. To create better large scale models of atmospheric and oceanic flows, it is necessary to understand how mixing occurs at sub-scale levels. A better understanding of how the coherent vortices, of two dimensional turbulent fields, effect mixing would therefore be useful.
The three dimensional case, in which the inverse cascade of energy from small to large scale, is hardly perceptible, cannot be used as an approximation for two dimensional one. It is this inverse cascade which is assumed to be responsible for the formation of coherent, long lived vortices that develop out of random turbulence.
The first aim of the experiment is to verify that the turbulent diffusion velocity in two dimension is infinitely greater than the measured in three dimensions. Secondly we will try to quantify the intermittent behavior of the vorticity fields, and finally we analyze the influence of the small scales and the long range memory.

To achieve these goals, the data obtained by this study will be analyzed in three ways:

- The first part of analysis is to show how the elements are retained in the long-term life of two kinds of interaction, the two- and the three-dimensional ones. This analysis will be called *Qualitative Universality*.
- Statistics analyses on velocity moments and velocity derivative moments, respectively. This phase of the study may be indicated as *large- and small Scale coherent structures*.
- In conclusion will be analyzed the *long-range memory* by measuring the time take to loose the memory of the initial condition.

After this brief introduction, the numerical experiment is described in more detail.
The two dimensional Navier-Stokes equations, that determine the flow motion, are numerically solved with a fully de-aliazed (3/2 rule) Fourier-Galerkin pseudo-spectral method. The computational domain is a $2\pi \times 2\pi$ rectangle with 1024×1024 points. In order to achieve maximum symmetry, it is advantageous not have *any* boundaries. We could thus assume that the fluid fills all of the space $\mathbb{R}^2$. The unboundness of the space does, however, lead to some mathematical difficulties. We shall therefore often assume *periodic boundary conditions* in space variable $\mathbf{r} = (x, y)$:

$$\mathbf{v}(x, y) = \mathbf{v}(x + nL, y + mL)$$

for all x, y and all signed integer n, m. Here L indicates the period. Therefore the computational domain is a rectangle with periodic conditions in all directions, see figure 3.1.

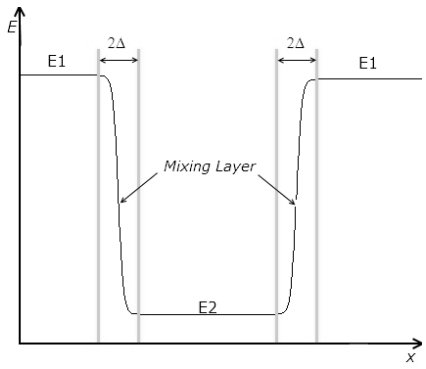

Figure 3.1: Scheme of the flow

In the scheme of the flow is immediate to observe a symmetry.
In the initial condition, the two isotropic turbulent fields are matched by means of a hyperbolic tangent function. This transition layer represent 1/80 of the longitudinal length 2π. The matched field is

$$\mathbf{u}(\mathbf{x}) = \mathbf{u}_1(\mathbf{x})p(x) + \mathbf{u}_2(\mathbf{x})[1 - p(x)]$$

where

$$p(x) = \frac{1}{2}\left[1 + \tanh\left(a\frac{x}{L}\right)\tanh\left(a\frac{x - L/2}{L}\right)\tanh\left(a\frac{x - L}{L}\right)\right]$$

The suffixes $1, 2$ indicate high- and low- energy side of the mixing respectively, x is the inhomogeneous direction, L is the width of the computational domain in the x direction. Constant a determines the initial mixing layer thickness Δ, conventionally defined as the distance between the points with normalized energy values 0.25 and 0.75 when the low-energy side is mapped to zero and the high-energy side to one. In this simulation $a = 28\pi$, so $\Delta(0) = 2\pi/80$. In this way the initial thickness is large enough to be resolved but small enough to have large regions of homogeneous turbulence during the simulations.
In the present study the ratio of the turbulent kinetic energies has been chosen as the sole control parameter. In particular, the following values of energy ratio were chosen:

$$6.6 \qquad 40 \qquad 300 \qquad 10^4 \qquad 10^6$$

All simulation are made with a diffusion coefficient equal to $0.244\ 10^{-9}\ [m^4/s]$.
In order to provide additional numerical details of the simulations the turbulence macroscales have been determined.
First of all, we must choose a discretization time step of need. We want to satisfy the CFL condition with a Courant number equal to 0.25. Assuming to have already made the equations dimensionless, we can put the maximum of velocity unitary, and therefore:

$$\frac{v_{max}}{\Delta x}\Delta t < 0.25 \quad \Leftrightarrow \quad \Delta t < \frac{0.25 \cdot 2\pi}{1024} \cong 0.0015$$

The time step was chosen so that fully satisfy this inequality. In particular we put $\Delta t = 5 \cdot 10^{-4}$, we are so sure of having a stable numerical method. We can also verify that our choice of discretization time step does not imply instability of the numerical method by looking at the time evolution of the Courant number, calculated as $c(t) = v_{max}(t)\Delta t/\Delta x$, and shown in figure

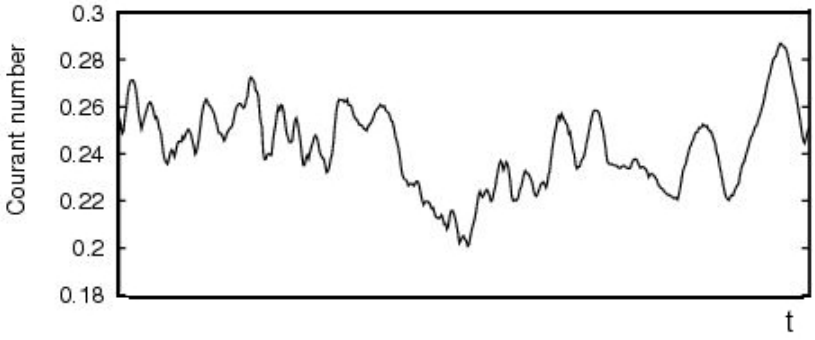

Figure 3.2: Time evolution of the Courant number

3.2. It's evident that the CFL condition is always fully satisfied, and also it always oscillates around the chosen value 0.25.
As length scale space can be considered the width of the mixing layer at the initial time, ie:

$$l = \frac{2\pi}{80} = 0.079$$

From this, we can derive the LETOT, large eddy turn-over time. Indeed, after normalization, the kinetic energy of the high energy field, is always 0.5, having raised unit the maximum velocity, and then:

$$\tau = \frac{l}{\sqrt{E_1}} = \frac{0.079}{\sqrt{0.5}} = 0.11$$

As $\tau/\Delta t$, it appears that the simulation of a LETOT requires 220 time steps. From some preliminary tests, it was seen that after about 23 time units mixing is complete and there is a situation similar to that sketched in figure 3.3 . But, for the purposes of this study, this situation is not useful, so we decided to make all simulations with 5000 time steps, equivalent to 22.72 time units.

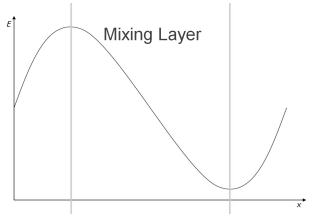

Figure 3.3: Interaction between the two mixing

3.1 Numerical method

To do these simulations, we used a two dimensional Navier-Stokes code. The code, written by Jost von Hardenberg, operates as shown in the following diagram.

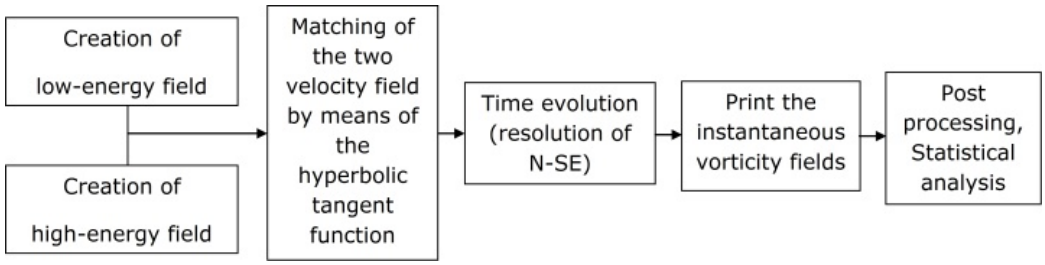

Figure 3.4: Code diagram

Same way as the three-dimensional case.
The initial condition is prepared initializing the flow using Fourier mode associated with the velocity field, fixing their amplitude to match a given spectrum and assigning them random phases. But the two dimensional Navier-Stokes code requires the the initial field to be in vorticity, unlike the three-dimensional program, which uses a velocity field. This creates an issue in using the hyperbolic function to create the energy gradient between the two fields, which required that the field be expressed as velocities. To solve this problem, a separate program was created that:

- accesses two vorticity fields already created with different average kinetic energies and vorticity distributions,
- converts the two vorticity fields into velocity fields and combines them using the hyperbolic function,
- reconverts the final combined velocity field back into a vorticity field.

After implementing the initial conditions, the program performs the time evolution of the vorticity field.
To understand how the code works, we have to begin by the equation. Consider the N-SE in 1.3. In a two-dimensional framework the incompressibility equation can be written $\partial_x u + \partial_y v = 0$, where (u, v) are the components of the velocity. According to the Schwartz theorem, there exist a stream-function ψ such that

$$u = \frac{\partial \psi}{\partial y} \qquad v = -\frac{\partial \psi}{\partial x}$$

or equivalent

$$\mathbf{u} = -\hat{\mathbf{k}} \times \nabla\psi \tag{3.1}$$

where $\hat{k}$ is a unit vector normal to the flow. The vorticity $\omega = \nabla \times \mathbf{u}$ is directed along the vertical axis. Taking the curl of 3.1, we find that the vorticity is related to the stream-function by a Poisson equation

$$\Delta\psi = -\omega$$

After this consideration we can rewrite the N-SE in the follow way:

$$\frac{\partial\omega}{\partial t} + \underbrace{\frac{\partial\psi}{\partial y}\frac{\partial\omega}{\partial x} - \frac{\partial\psi}{\partial x}\frac{\partial\omega}{\partial y}}_{J(\psi,\omega)} = \nu\Delta\omega$$

where $J(\psi, \omega)$ indicates the Jacobian, or non-linear therm. If we pass to the spectral space, i.e if we do an Fourier transformed, this equation become

$$\frac{d}{dt}\hat{\omega} + \hat{J} = -\nu k^2\hat{\omega}$$

where $k^2 = k_x^2 + k_y^2$ is the wave vector module. By performing some simple algebraic passage, we see how we can integrate exactly the diffusive term. In fact, rearranging the equation and multiplying both sides by $e^{-\nu k^2 t}$, we yield:

$$\frac{d}{dt}\left(\underbrace{e^{+\nu k^2 t}\hat{\omega}}_{\hat{\zeta}}\right) = -\hat{J}e^{-\nu k^2 t} \qquad \Rightarrow \qquad \frac{d}{dt}\hat{\zeta} = -\hat{J}e^{-\nu k^2 t}$$

The time integration is done by means of a third-step third-order Adams-Bashforth method.
To complete this brief description of the numerical method we have yet to see how it is treated the nonlinear term and how to avoid aliasing phenomenon.

Let'start with the non linear term. First we evaluate the velocity $(u, -v)$ from the vorticity in the Fourier space in this way

$$\hat{u} = -\frac{ik_y}{k^2}\hat{\omega} \qquad \hat{v} = \frac{ik_x}{k^2}\hat{\omega}$$

Then we call the FFT inverse to return in the physical space and so we can calculate the products $p_1 = u\omega$ and $p_2 = v\omega$. Then we can call the FFT for p_1 and p_2 and finally we can compute the Jacobian as follows

$$\hat{J} = ik_x\hat{p}_2 - ik_y\hat{p}_1 \tag{3.2}$$

We can now consider the aliasing problem. The key to this de-aliasing technique in the use of a discrete transform with M rather than N points, where $M \geq 3N/2$. For understand what happens we can restrict at an one dimensional problem. Let be

$$y_j = \frac{2\pi}{M} j \qquad \bar{u}_j = \sum_{k=-M/2}^{M/2-1} \tilde{u}_k^{iky_j} \qquad \bar{v}_j = \sum_{k=-M/2}^{M/2-1} \tilde{v}_k^{iky_j}$$

We want to compute $\bar{s}_j = u_j v_j$ for $j = 0, 1, \ldots, M-1$, where

$$\hat{u}_k = \begin{cases} \hat{u}_k, & |k| < N/2 \\ 0 & \text{otherwise} \end{cases}$$

Similarly, let

$$\tilde{s}_k = \frac{1}{M} \sum_{k=-M/2}^{M/2-1} \bar{s}_j e^{-iky_j}, \qquad k = -\frac{M}{2}, \ldots, \frac{M}{2} - 1$$

Then

$$\tilde{s}_k = \sum_{m+n=k} \tilde{u}_m \tilde{v}_n + \sum_{m+n=k\pm M} \tilde{u}_m \tilde{v}_n$$

We are only interested in $\tilde{s}_k$ for $|k| \leq N/2$, and choose M so that the second term on the right-hand side vanishes for these k. Since $\tilde{u}_m$ and $\tilde{v}_m$ are zero for $|m| > N/2$, the worst case condition is

$$-\frac{N}{2} - \frac{N}{2} \leq \frac{N}{2} - 1 - M \qquad \Rightarrow \qquad N \leq \frac{2M}{3} + 1$$

For this reason, after each FFT, we truncate our spectral field with a truncation ratio equal to 0.67. To learn more see [1].

The output of the code is a series of vorticity field. The instantaneous vorticity are printed every 25 time steps or 2.75 time units.
Finally, any result is ensemble averaged over 100 samples and the anisotropy and intermittency of velocity is observed.

3.2 Simulation results and discussion

The initial conditions place a kinetic energy gradient in the direction of inhomogeneity, here denoted x.
The gradient results from the different levels of kinetic energy of the two interacting turbulence fields and the only parameter that are actually controlled in the experiment are the ratio of energy $\mathcal{E} = E_1/E_2$.

This kind of mixing is characterized by the absence of a mean shear, so that there is no production of turbulent kinetic energy and no mean convective transport. The turbulence spreading is caused only by the fluctuating pressure and velocity field. See the flow visualization in figure 3.5.

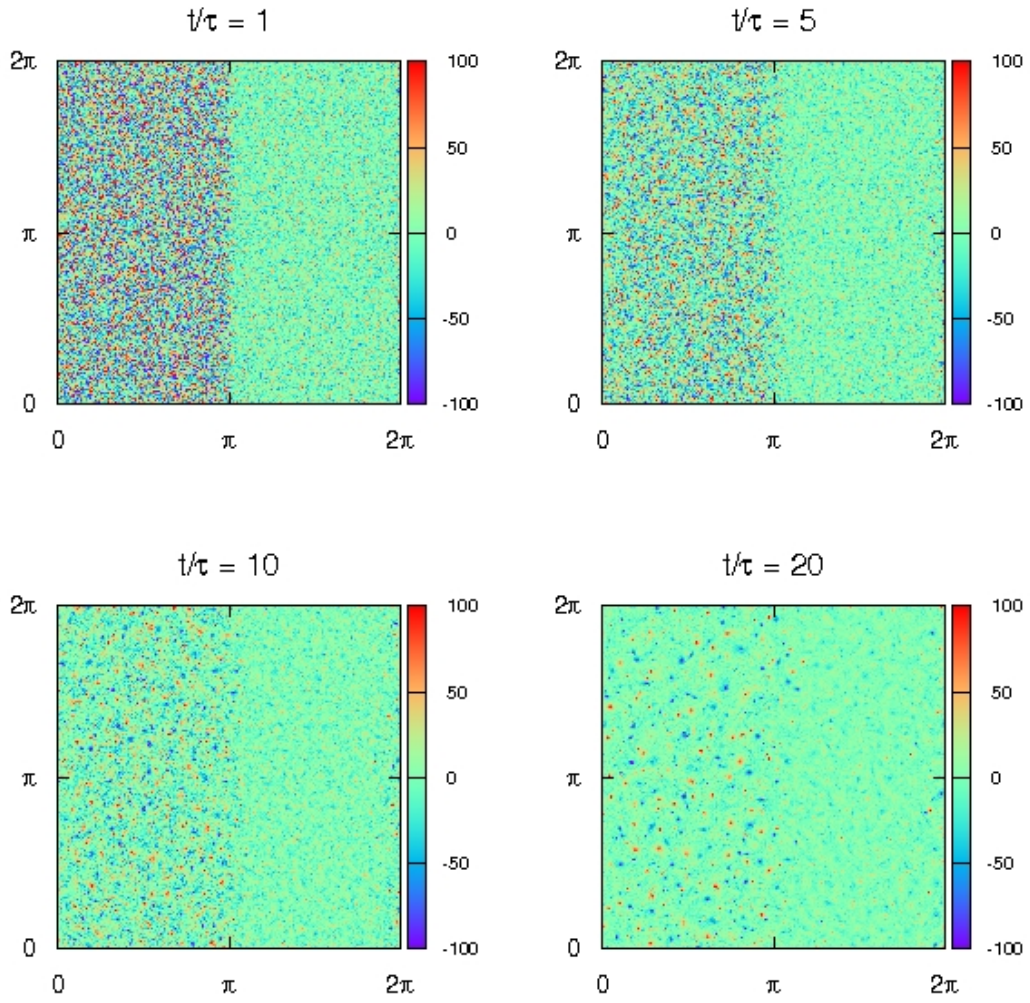

Figure 3.5: Visualization at four time instants of vorticity contours with energy ratio 6.6

The behavior of the mixing is well illustrated in the figure below that shows the trend of energy profiles at different instants of time and with different values of $\mathcal{E}$.

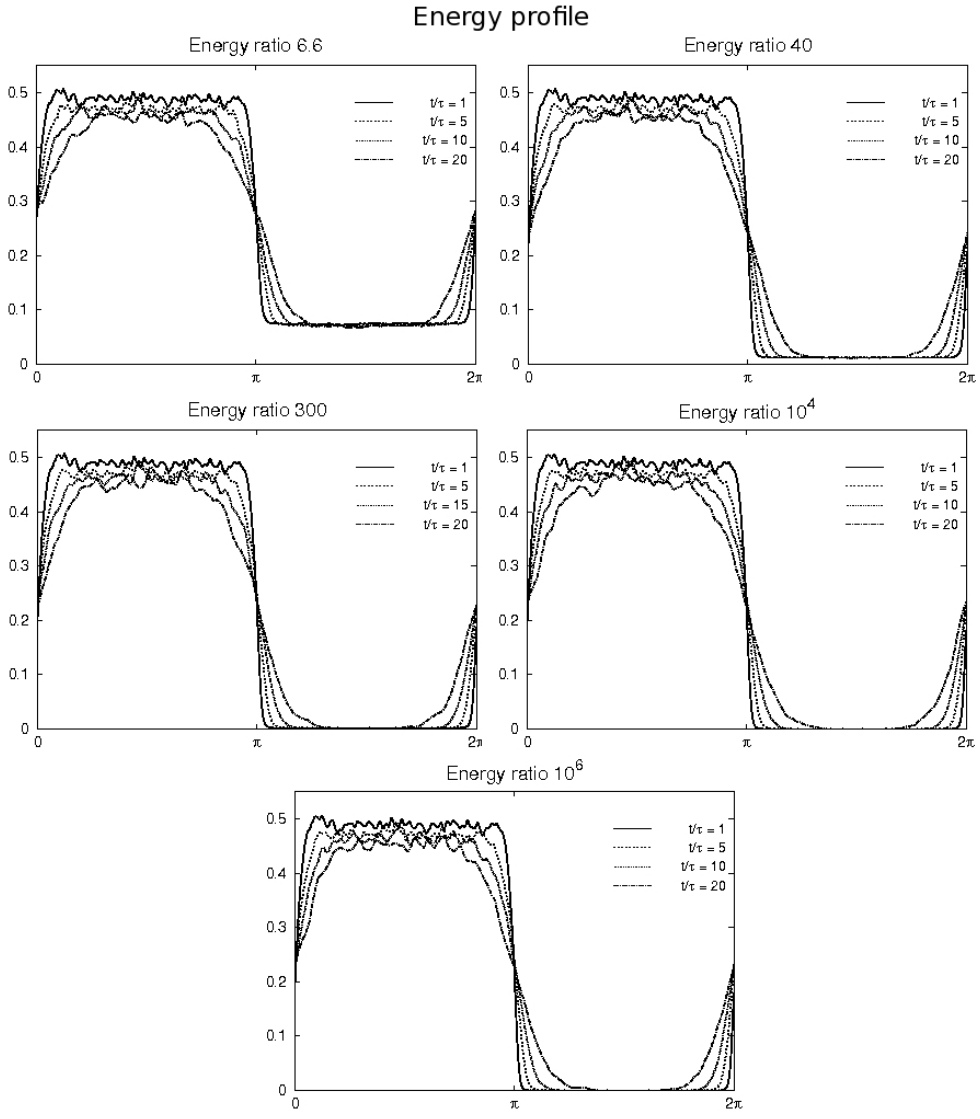

Figure 3.6: Normalized kinetic energy profile at four time instant

Analysis of the results was carried out following the scheme mentioned in the previous paragraph.
We will start by comparing the evolution of mixing achieved in two and three dimensions.

3.2.1 Qualitative Universality

As mentioned, the three dimensional case cannot be used as an approximation for the two dimensional one, now we will show some results that confirm the stronger influence of the inverse energy cascade in the flat case.
Figure 3.7 shows the time evolution of the velocity field for the corresponding three dimensional experiment in a $2\pi \times 2\pi \times 4\pi$ analytical domain and with energy ratio 6.7.

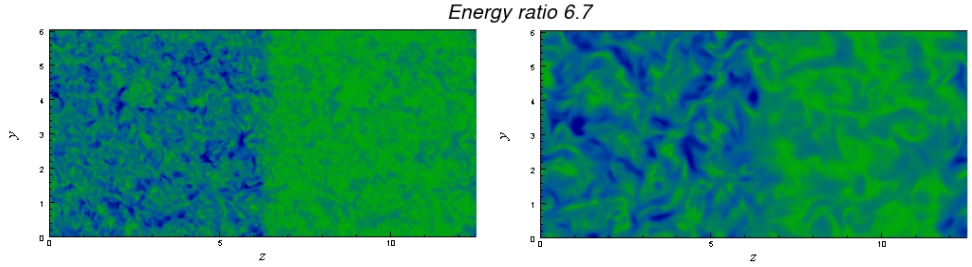

Figure 3.7: Initial and final velocity field for the corresponding three dimensional experiment with $E_1/E_2 = 6.7$

In both experiments, the energy and the integral scale are normalized by the values of the high energy field, while the spatial coordinate is normalized by the length Δ. The function Δ is defined by mapping the low energy side of the mixing layer to zero and the high energy side to one, and it is equal to the distance between the points with energy values 0.25 and 0.75. It should be noticed that by doing so, the energy gradient value, is defined as $(E_1 - E_2)/2\Delta$.
The evolution of the thickness of mixing layer is a quantity important to the evolution of the flow. Previous studies have led to estimate the asymptotic behavior of this thickness for the three-dimensional case, yielding the following results:

$$\frac{\Delta(t)}{\Delta(0)} \propto \frac{t}{\tau}^{0.43}$$

What happens to the current case is instead shown in figure 3.8

It is interesting to observe that, with increasing time, all the results collapse on a single curve. By executing a best fit, we estimate an asymptotic behavior exponential with a slope equal to 0.7226.
Therefore, in two dimensions, the mixing is developing quickly. This result is shows in figure 3.9, where we compare the asymptotic behavior of the types of mixing with two different values of the ratio of energy.

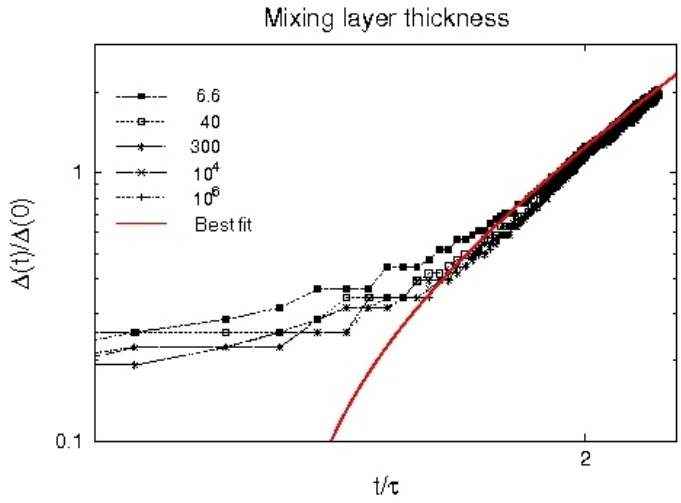

Figure 3.8: 2D mixing layer thickness as a function of the normalized time for the different values of $\mathcal{E}$, in log-log scale

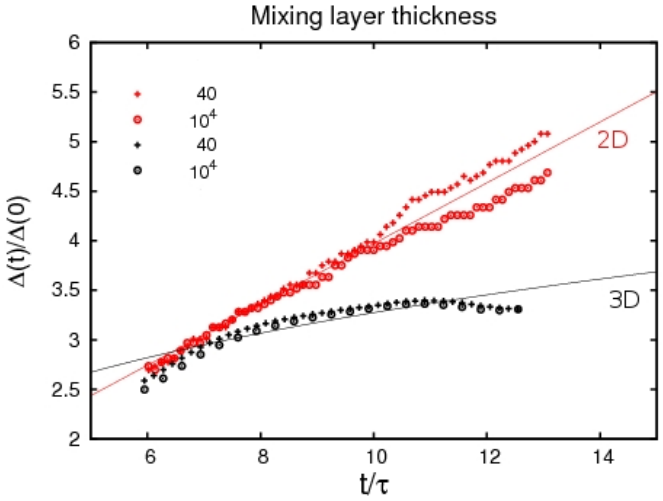

Figure 3.9: Comparison between the asymptotic behavior of the thickness mixing layer in 2D and in 3D

During the evolution of the flow, the region of high energy spreads in the other, thereby increasing the mixing layer. Also we can see how the mixing layer as a region of large variance diffusing into a region of lower variance. In this spirit we can define the *penetration* as the position of the maximum of the skewness ($S = \langle u^3 \rangle / \langle u^2 \rangle^{3/2}$) normalized over the mixing thickness $\Delta(t/\tau)$

$$\eta = \frac{x_s}{\Delta(t/\tau)}$$

Asymptotically in time we have $\eta = \eta(\mathcal{E})$ and the two trends are shown in figure 3.10

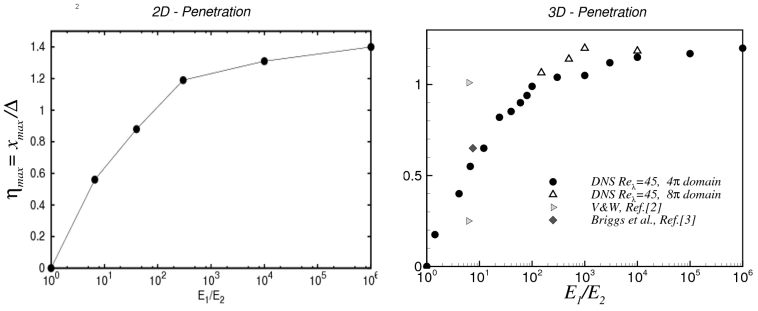

Figure 3.10: 2D and 3D penetration. Asymptotic behavior with the mixing layer kinetic energy ratio

Especially for applications in geophysics, it is very important to study how varying the turbulent diffusion velocity downgrading to 2 dimensions. In this context it makes sense to define the rate of diffusion as the time derivative of the maximum of the skewness. We have:

$$2D : v_{\mathcal{D}} = \frac{dx_s}{dt} = \eta \frac{d\Delta}{dt} = \frac{\eta}{\tau} \frac{d \, \frac{t}{\tau}^{0.722} t}{dt} \propto t^{-0.28}$$

$$3D : v_{\mathcal{D}} = \frac{dx_s}{dt} = \eta \frac{d\Delta}{dt} = \frac{\eta}{\tau} \frac{d \, \frac{t}{\tau}^{0.43}}{dt} \propto t^{-0.57}$$

Then asymptotically in time

$$\frac{v_{\mathcal{D},2}}{v_{\mathcal{D},3}} \approx \frac{t^{-0.28}}{t^{-0.57}} = t^{0.29} \to \infty$$

Therefore in two dimensions, asymptotically in time, the turbulent diffusion is infinitely greater than that measured in three dimensions.

3.2.2 Large- and Small-Scale coherent structures

In this section we consider the asymptotic behavior with regards to the variation of the parameter that controls this kind of shearless mixing layer, that is the initial energy ratio $\mathcal{E}$ between the high-energy turbulent field and the low energy one.
The two external fields show, for moderate values of $\mathcal{E}$, decay exponents which are very close, so that the two homogeneous turbulence external to the mixing decay in a similar way and the value of E_1/E_2 remains quite constant during the time interval considered [14]. After few initial eddy turnover time a true mixing layer begins to emerge from the initial condition and reaches a self similar state. This means that all normalized moment distribution across the mixing collapse to a single curve when the position is normalized with the mixing layer thickness.
The results show that the mixing layer is highly intermittent in the self similar stage of decay: so similarly to the case 3d [15], the experiment shows that the presence of a turbulent energy gradient is sufficient for the appearance of intermittency and anisotropy.
In order to study the flow intermittency, moments of the longitudinal velocity component were computed. The velocity fluctuation u is responsible for the energy transport across the mixing. The skewness distribution is indicative of asymmetry between the positive and negative fluctuations is a principal indicator of intermittent behavior. We define $S(x) = \left\langle \bar{u^3} \right\rangle / \left\langle \bar{u^3}^{3/2} \right\rangle$. Because a Gaussian distribution is symmetric, its skewness is identically zero. In other word, it vanishes in homogeneous isotropic turbulent flows and thus it remains close to zero in the fields external to the mixing while takes a positive value within the mixing layer. Figure 3.11 shows the skewness in four different instants of time for each energy ratio considered.

During the initial eddy turnover times the skewness increases steadily, before bending at a normalized time varying from 5 to 10. At this point the mixing layer enters a near self-similar stage of evolution. Figure 3.12, shows the maximum skewness inside the mixing layer as a function of time and as a function of $\mathcal{E}$.

The intermittent flow may also be analyzed by looking at the fourth moment of u. The Kurtosis ($K = \left\langle \bar{u^4} \right\rangle / \left\langle \bar{u^2}^2 \right\rangle$) is a measure of whether the data are peaked or flat relative to a normal distribution. It is constant and equal to three in homogeneous isotropic turbulent flow. Figure 3.13 shows the kurtosis in four different instants of time for each energy ratio considered.

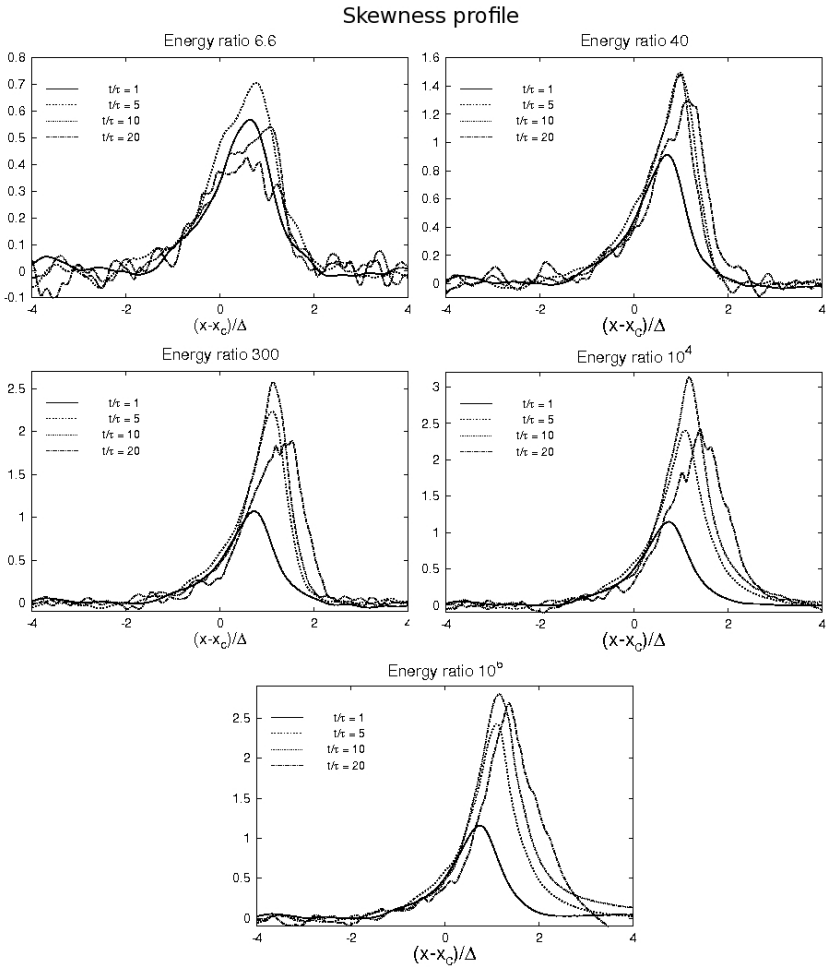

Figure 3.11: Skewness of the velocity component in the inhomogeneous direction for each energy ratio. x_c is the mixing layer centre and Δ is the mixing layer thickness

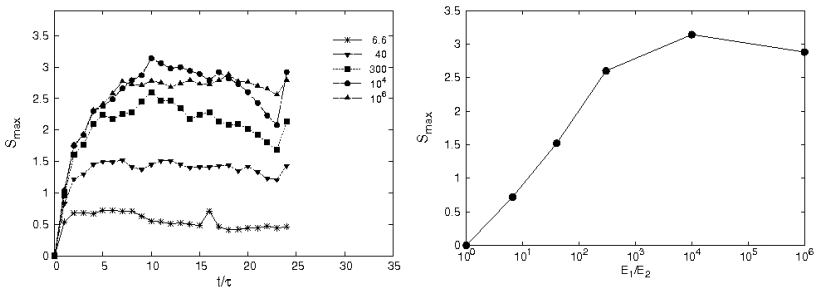

Figure 3.12: Maximum of the skewness

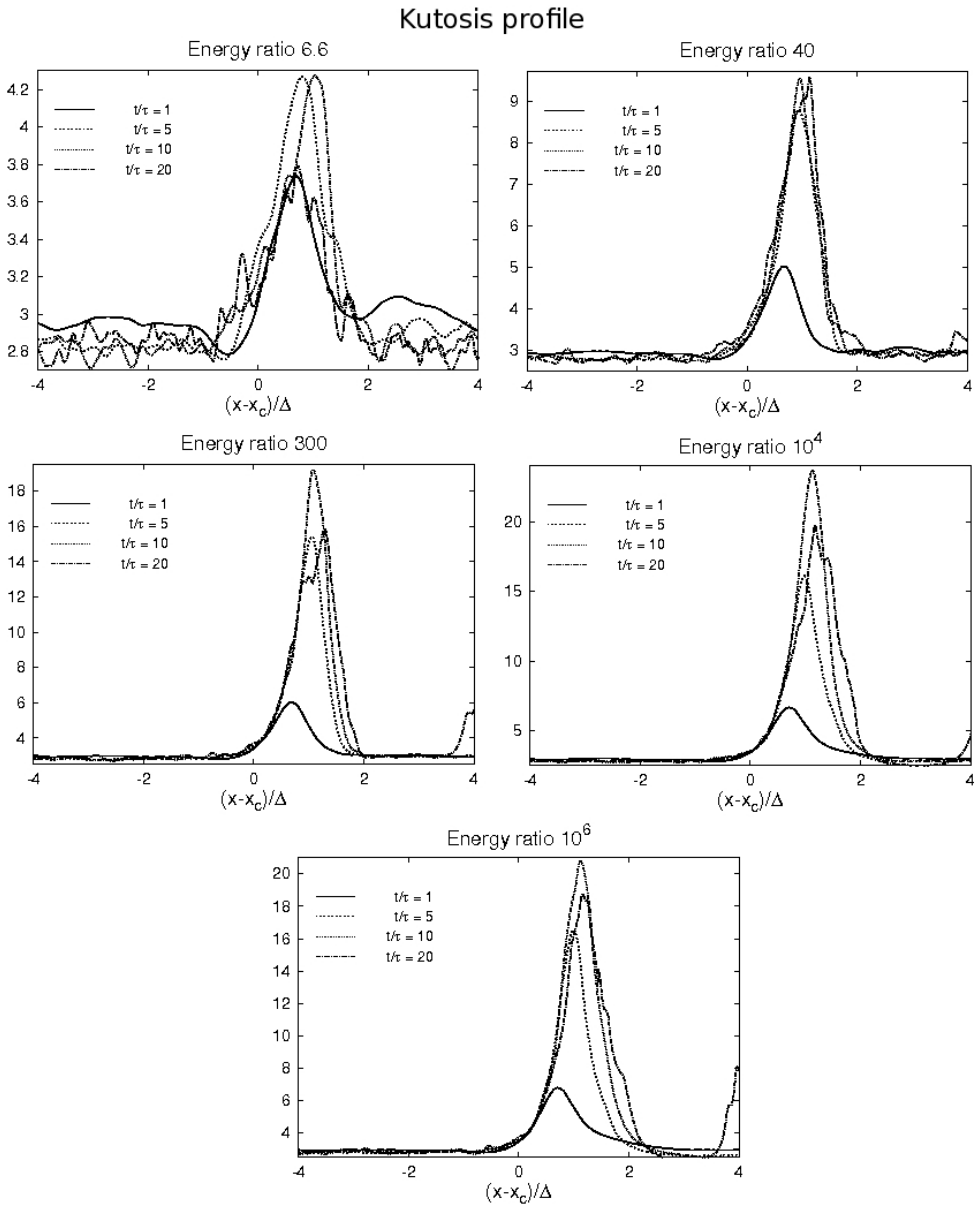

Figure 3.13: Kurtosis of the velocity component in the inhomogeneous direction for each energy ratio. x_c is the mixing layer center and Δ is the mixing layer thickness

In figure 3.14 we show the maximum kurtosis inside the mixing layer as a function of time and as a function of E_1/E_2. There is a peak followed by a decrease, that could be interpreted as the fact that the more extreme intermittent turbulent events take place at the end of the formation time interval where the mixing process develops and before the self-similarity sets in. from the distribution of the peak of kurtosis inside the mixing, it can be noted that it reaches very high values, much higher than three. In fact the kurtosis asymptotic value is about 20 and indicates the presence in mixing layer of extremely intense intermittent events.

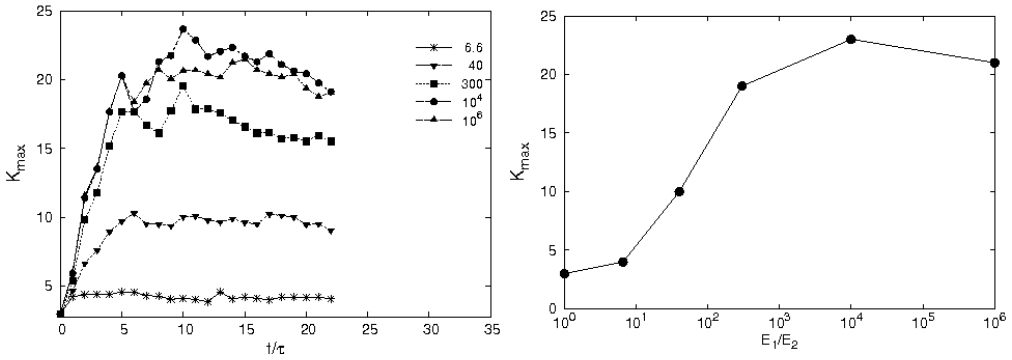

Figure 3.14: Maximum of kurtosis

In conclusion, all the mixing simulated show a departure from a Gaussian state for any turbulent energy ratio and the intermittency is high dependent on the turbulent energy ratio between the two interacting flow.

3.2.3 Long-range memory

When we speak of long range memory, we can interpret it as the time in which the solution "forgets" the initial condition. To get an estimate of this, we need to use a probabilistic description of turbulence even if we know that the basic equation, N-SE, is deterministic, as we have anticipate in section 3.1.
To better understand what justifies this description we can start from an example. In figure 3.15 The mean flow does not exist so that the signal

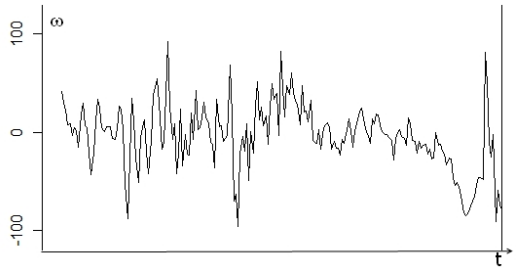

Figure 3.15: Time evolution of the vorticity in a fixed point

appears to fluctuate around zero. When we look at this signal we can note that:

- The signal appears highly disorganized and present structure an all scale
- The signal appears unpredictable in its detailed behavior
- Some proprieties of the signal are quite reproducible

The first point has been amply dealt with in chapter 1 and 2. Regarding the last point, one instance of a reproducible property is the histogram. As shown in figure 3.16

The second point is what we want to use here. Since we cannot predict the detailed behavior of the vorticity we can consider its time evolution in each fixed point like a time series or a discrete stochastic process, i.e we can consider it like a sequence of random variables. In other words we can use some probabilistic tools to estimate the long time behavior. We then selected some points of our analytical domain and recorded the values assumed by vorticity in this at all the time. For each value of energy ratio, we have 50 achievements. Combining all the 50 time evolution for each point, we then have a data set large enough to make a good statistical analysis in term of time series.

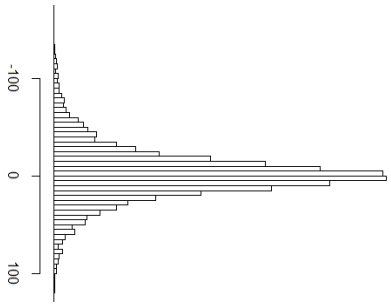

Figure 3.16: Histogram of the signal in the previous figure

Now we can evaluate the *autocorrelation function*. The autocorrelation function is defined as

$$\rho(t) = \frac{\langle \omega(0)\ \omega(t) \rangle}{\langle \omega(0)^2 \rangle}$$

This is a measure of how much the vorticity at time t is influenced by its initial value.
As a first important result we have that the autocorrelation function does not depend on points selected.

The graph in figure 3.17 shows the autocorrelation function, obtained as described above, for each energy ratio considered.

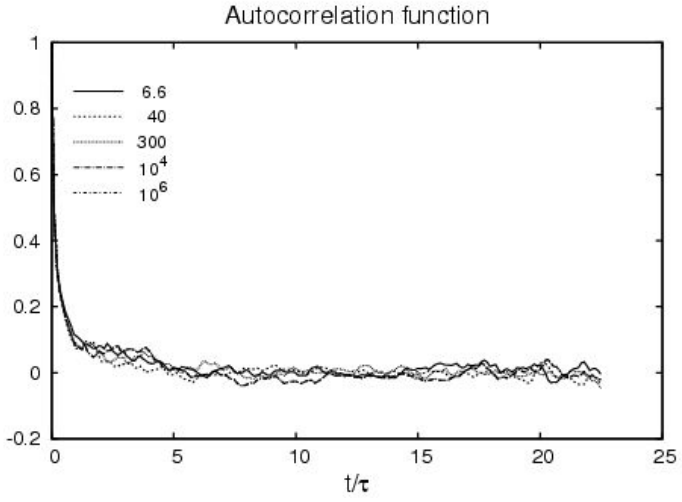

Figure 3.17: Autocorrelation function for each energy ratio

All the curves collapse into one, and this shows that the long-range memory does not depend on the energy ratio.

Then we can simply see more in detail only one of these functions. The following figure shows the values of the correlations for E=6.6

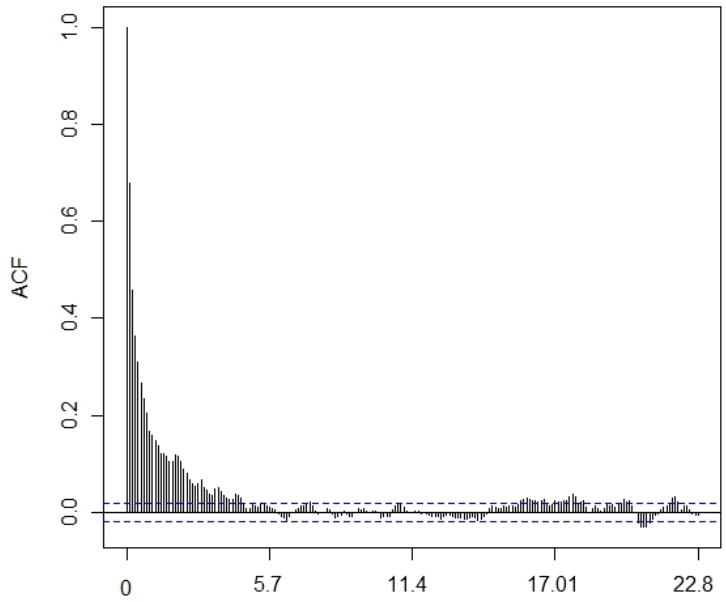

Figure 3.18: Autocorrelation function for the energy ratio 6.6

We can observe how, even after 20 time units, there is not total independence of the data from the initial value, since the autocorrelation function is still 3%.

Finally we can try to interpolate the evolution of these curves.
The trend of these curve, in fact, discriminates whether we are dealing with phenomena of short- or long-range dependency. The Long-range dependency relates to the rate decay of statistical dependence, with the implication that this decays more slowly than an exponential decay, typically a power-like decay.
We have found that the function that best fits their trend is

$$\frac{a}{((t/\tau)+b)^c}$$

where the fitting parameters are:

$$a = 0.123662 \pm 0.002115 \qquad (1.71\%) \qquad b = 0.0761417 \pm 0.005588 \qquad (7.339\%)$$

$$c = 0.811268 \pm 0.02204 \qquad (2.717\%)$$

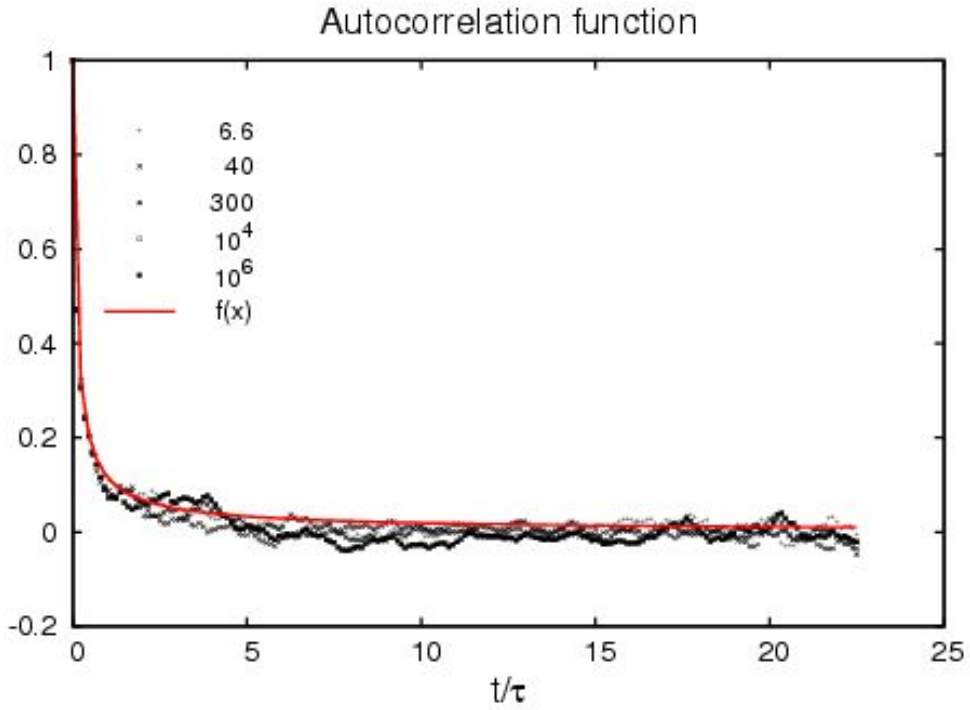

Figure 3.19: Fitting of the statistical dependence

In other words our autocorrelation function goes as $t^{-0.8}$ In figure 3.19 we show the actually autocorrelation function and the with the estimated one to give a visual comparison.

In conclusion we can therefore speak of long-range dependency.

Chapter 4

Stratified flow

The name stratified flow is applied to a flow primarily in the horizontal direction that is affected by a vertical variation of the density. Such flows are of considerable importance in geophysical fluid mechanics. The obvious case of the effect of vertical temperature variations on the wind near the ground is only one of a number of examples in the atmosphere, and the effects of both temperature and salinity variations play an important role in many aspects of dynamical oceanography.
The density may, in general, either increase or decrease with height. The former case gives rise to an interaction between the mean flow and the convection that would occur in the absence of mean flow. However, in this chapter we are primarily concerned with the case of stable stratification, that is to say the density decreases with height.
Vertical motions then tend to carry heavier fluid upwards and lighter fluid downwards, and are thus inhibited. This inhibition may take the form of modifying the pattern of the laminar motion or of preventing or modifying its instability. We require a quantitative criterion for this to be a strong effect.
Since most of the experiments on stratified flows have used salt rather than heat as the stratifying agent we shall retain the density variations explicitly, rather than relating them to temperature variations.
In the next section we will see how obtain simplified equations for stratified flows. In section 4.2 we will give a mathematical justification for the concept of stable stratification. In 4.3 we will define the dimensionless parameter for this kind of flows: the Froude number. and finally in the last section we will introduce the internal waves, that are wave motion due to the tendency for the vertical motion to be suppressed.

4.1 The Boussinesq approximation

The processes that can lead to changes in air density in the atmosphere are in principle three: the variation of atmospheric pressure with height, the pressure changes that occur dynamically because of atmospheric motions, the phenomena of thermal expansion. Consider separately the three effects. The first effect and phenomena associated with stratification and correspond to the budget in the N-SE between the vertical components external forces and pressure

$$\nabla P = f^{ext}$$

leading to the equation of hydrostatic balance.
The second and third effect corresponds to density fluctuations generated in a dynamics due to motions of fluid and temperature variations. Imagine an area of medium size $\approx L$ whose speed and its variation are both $\approx U$. This means that the corresponding time scale is $\approx L/U$. In the absence of external forces and viscous terms in Navier-Stokes will therefore order of magnitude, in sequence:

$$\frac{U}{\tau} \approx \frac{U^2}{L} \approx \frac{\Delta P}{\rho L}$$

where Δp is the change in pressure corresponding. From the equation of state we have

$$P = \rho \frac{T}{m} \approx \rho v_{th}^2 \qquad \Rightarrow \qquad \frac{\Delta P}{\rho} \approx v_{th}^2 \frac{\Delta \rho}{\rho} + \frac{\Delta T}{m}$$

Therefore, replacing the previous one, we get

$$\frac{\Delta \rho}{\rho} < \max\left(\frac{u^2}{v_{th}^2}; \frac{\Delta T}{T}\right)$$

Recall that in less than a factor $\mathcal{O}(1)$, v_{th} is the speed of sound c_s for an ideal gas. We thus see that if the Mach number $M = u/c_s$ and the relative variation of the temperature scale $\Delta T/T$ are both small, the density variations produced are themselves small, ie, the motion of fluid will be to a first approximation incompressible. In the troposphere, the first condition is always verified and the only effect that produces changes in density is the stratification.
Therefore, atmospheric motions, with a much smaller vertical scale height of the troposphere, will be in good approximation incompressible. In the atmosphere, things are more complicated, since changes in temperature are associated with density variations, and even if the motions occur at scales

much smaller than the height of the troposphere, and are in good approximation incompressible, small density variations produced are still responsible for the same motion through convection. These effects can be taken into account as perturbations, through the so-called *Boussinesq approximation*.

The Boussinesq idea consist in take into account the density fluctuation just in the term in which it is absolutely necessary, while consider it as a constant for all the others. To understand what this means we have to do an relative analysis magnitude.
First we can consider the continuity equation:

$$\frac{1}{\rho}\frac{D\rho}{Dt} + \frac{\partial u}{\partial x} + \frac{\partial v}{\partial y} + \frac{\partial w}{\partial z} = 0$$

It is always possible see the density as a constant plus a time dependent correction term

$$\rho(x, y, z, t) = \rho_0 + \rho'(x, y, z, t)$$

where the fluctuation ρ' is related to the temperature effect. Now, since ρ_0 is a constant, we have $D\rho/Dt = D\rho'/Dt$.
Furthermore, in the absence of other information, we assume that the typical values given by the derivatives of $\bar{u}$ are approximately equal. It is also reasonable to assume that the velocity of the fluid remains limited: a particle of fluid that moves at speeds arbitrarily large unlimited kinetic energy, and this seems physically unreasonable. If we indicate with U the typical amplitude of fluctuations of speed and we call L the typical distance between its maximum and its minimum, we venture to say that the typical value of the derivative space of

The hypothesis most daring of this reasoning is assuming that

$$\Delta t \approx \frac{L}{U}$$

If this hypothesis is reasonable, we can proceed with the magnitude analysis. In fact we have

$$\left|\frac{D\rho'}{Dt}\right| \approx \frac{\Delta\rho'}{\Delta t} \approx \frac{\Delta\rho' U}{L}$$

Moreover $\rho \approx \rho_0$ and then

$$\frac{\left|\frac{1}{\rho_0}\frac{D\rho'}{Dt}\right|}{\left|\frac{\partial u}{\partial x}\right|} \approx \frac{\frac{\Delta\rho' U}{\rho_0 L}}{\frac{U}{L}} = \frac{\Delta\rho'}{\rho_0} << 1$$

That is, the term containing the density is small compared to the term containing the speed as much as it is ρ' with respect to the reference density ρ_0. In other words, in the equation of continuity, the density is dominated by the divergence of the velocity and thus, approximating, we can use the equation of mass conservation for incompressible fluids:

$$\nabla \cdot \mathbf{u} = \mathbf{0}$$

Let us now turn to the equation. Suppose that there is no motion and that the density is constant. In this case the pressure gradient is given by the hydrostatic equation

$$\frac{\partial p_0}{\partial z} = -\rho_0 g$$

We can now express the pressure in the presence of motion and density fluctuations as the sum of hydrostatic pressure p_0 and a dynamic pressure p'

$$p(x, y, z, t) = p_0(z) + p'(x, y, z, t)$$

Simply replacing the Navier Stokes equation is obtained

$$(\rho_0 + \rho')\left(\frac{\partial \mathbf{u}}{\partial t} + \mathbf{u} \cdot \nabla \mathbf{u}\right) = -\nabla p' - \underbrace{\left(\frac{\partial p_0}{\partial z} + p_o g\right)}_{=0} - \rho' g \hat{k} + \nu \Delta \mathbf{u}$$

The hydrostatic terms cancel each other, then the density is only two terms. On the left side the total density multiply the acceleration term. Since by hypothesis $(\rho_0 + \rho') \approx \rho_0$ we are allowed to disregard ρ'. To the right of the term representing the forces of gravity only has the density fluctuations. In this case we can not ignore ρ', because this would be to completely eliminate the effect of gravity in our equations. Therefore the N-SE in approximating Boussinesq are written in this form:

$$\begin{aligned} &\nabla \cdot \mathbf{u} = \mathbf{0} \\ &\rho_0 \left(\frac{\partial \mathbf{u}}{\partial t} + \mathbf{u} \cdot \nabla \mathbf{u}\right) = -\nabla p' - \rho' g \hat{k} + \nu \delta \mathbf{u} \end{aligned}$$

Summarizing, in the Boussinesq approximation, variations of all fluid properties other than the density are ignored completely. Variations of the density are ignored except insofar as they give rise to a gravitational force.

4.2 Stratification and the concept of static stability

We now want to understand under what conditions the gravity forces produce motion in a fluid.
To do this we assume that the flow is in absence of motion ($\mathbf{u} = \mathbf{0}$) and that we can apply the Boussinesq approximation. In this way, the equations are reduced to only the hydrostatic relation:

$$\frac{\partial p}{\partial z} = -\rho g \tag{4.1}$$

Suppose further that ρ depends only by z.
To determine if the vertical profile of density specified by $\rho(z)$ is stable or unstable, suppose we move a fluid particle from its initial height z at $z + h$. The equation which give us the vertical velocity of the particle is

$$\frac{Dw}{Dt} = -\frac{1}{\rho_0}\nabla p - \frac{\rho(z)}{\rho_0} g \tag{4.2}$$

For the moment we neglect the viscosity term, but just for simplifying the calculation. If we suppose to known $\rho(z)$, this equation contains two unknowns: w and p. In general, therefore, is not resolvable, but in our situation we can find an approximate solution. In fact, if the vertical velocity is initially zero the pressure is specified by the hydrostatic equation. Also until w remains small, we can use 4.1 to remove the pressure from 4.2 without entailing an appreciable error. In this way we yield:

$$\frac{Dw}{Dt} = -\frac{g}{\rho_0}[\rho(z + h) - \rho(z)]$$

It is important to note that the pressure term has led $\rho(h + z)$, because that is the hydrostatic pressure at the height at which the particle was increased, while the gravity term keeps $\rho(z)$ because we assume that during his motion the particles maintains its density. Now, Dw/Dt is the Lagrangian acceleration of the particle, so we have

$$Dw/Dt = d^2h/dt^2$$

Also note thate $\rho(z+h) - \rho(z) \approx d\rho/dz\ h$. Then we can rewrite our equation as follows

$$\frac{d^2h}{dt^2} - \frac{g}{\rho_0}\frac{d\rho}{dz}h = 0 \tag{4.3}$$

Is usual to define the quantity

$$N^2 = -\frac{g}{\rho_0}\frac{d\rho}{dz}$$

it is positive if the density decreases upward and negative otherwise. Until the displacement h of the particle is small is easy to solve this equation, because in this case is reasonable to consider $d\rho/dz$ as a constant. Some particular solution are almost obvious. It is easy to verify that if N^2 is positive, then both $h(t) = \cos(Nt)$ and $h(t) = \sin(Nt)$ satisfy the equation 4.3. These are periodic solutions, then the fluid particle, deviated from its initial position, not goes away from it, but it fluctuates around.
If, instead, N^2 is negative, we define $\mathcal{N} = \sqrt{-N^2}$; a pair of particular solutions is given by $h(t) = exp(\mathcal{N}t)$ and $h(t) = exp(-\mathcal{N}t)$. The first tells us that the displacement of the fluid particle increases indefinitely in time, and it no return to its initial position.

So we have found our "stability criterion" of the fluid:

- *Statistically stable fluid*, $N^2 > 0$ density decrease upward. A fluid particle oscillates if it deviated from its equilibrium position. The approximation made to write 4.3 are still valid.

- *Statistically unstable fluid*, $N^2 < 0$ density increase upward. A fluid particle moves away indefinitely from its initial position as soon as any perturbation deviate from it. The approximations made to write 4.3 are valid only in the first moment after the disturbance.

If the fluid is statically stable, the quantity N is the frequency of oscillations performed by the fluid particle around its position. It is known as *frequency of Brunt-Vaisala*

4.3 The Froude number

We consider the case of a three-dimensional flow outside boundary layers at high Reynolds and Peclet numbers, so that both viscous and diffusive processes are negligible. Thus we write the momentum and density equations (for steady flow)

$$\rho\mathbf{u}\cdot\nabla\mathbf{u} = -\nabla\mathbf{p} + \rho\mathbf{g} \tag{4.4}$$

$$\mathbf{u}\cdot\nabla\rho = \mathbf{0} \tag{4.5}$$

We take z vertically upwards and suppose that the basic stratification consists of a uniform density gradient $(-d\rho, /dz)$. Because ρ_0, does not vary

horizontally, the balance between $\rho_0 \mathbf{g}$ and the hydrostatic pressure can be subtracted out from equation 4.4 just as it can for an entirely uniform density.

We now consider, superimposed on this basic configuration, a flow with length and velocity scales L and U, produced, for example, by moving an obstacle of size L horizontally through the fluid at speed U. This will produce a modification of the density field which we denote by ρ', related to the stratification by equation 4.5 in the form

$$\mathbf{u} \cdot \nabla \rho' + \mathbf{w} \frac{\mathbf{d}\rho_\mathbf{0}}{\mathbf{dz}} = \mathbf{0} \tag{4.6}$$

In order of magnitude

$$\rho' \approx \frac{WL}{U} \left| \frac{d\rho_0}{dz} \right| \tag{4.7}$$

W is now restricted by the fact that the flow cannot produce buoyancy forces associated with ρ' that are larger than the other forces involved. Since the buoyancy force does not contribute directly to the horizontal components of 4.4 it is convenient to work in terms of the vorticity form of this equation

$$\rho(\mathbf{u} \cdot \nabla \omega - \omega \cdot \nabla \mathbf{u}) = -\mathbf{g} \left(\hat{\mathbf{i}} \frac{\partial \rho'}{\partial \mathbf{y}} - \hat{\mathbf{j}} \frac{\partial \rho'}{\partial \mathbf{x}} \right) \tag{4.8}$$

Since the order of magnitude of ω is U/L this indicates that the order of magnitude of ρ' must remain not greater than

$$\rho' \approx \frac{\rho_0 U^2}{gL}$$

Comparison of this with 4.7 indicates that

$$\frac{W}{U} \approx \frac{\rho_0 U^2}{gL^2} \left| \frac{d\rho_0}{dz} \right| = Fr^2 \tag{4.9}$$

When Fr^2 is small the horizontal motion has only much weaker vertical motion associated with it. Fr is called *Froude number*, $1/Fr^2$ is sometimes known as the *Richardson number*.

Similar analysis can be given for flows in which viscous and/or diffusive effects are strong. This is a matter of some complexity, since different detailed treatments are appropriate for low, intermediate and high Prandtl number. Thus we omit consideration of it; when we talk below of low Froude number flows, it is assumed that any other criterion for the flow to be strongly constrained by stratification is also fulfilled.

Often low Froude number motion can be considered to be entirely two-dimensional in horizontal planes. In general we can have three situations:

- $Fr \to \infty$, g = 0, non stratified flow,
- $Fr \to 0$, strong stratification,
- $Fr \approx 1$, intermediate case

4.4 Internal waves

Stratified fluids can support a variety of types of wave motion, which have no counterparts in unstratified fluids. The reason is basically the tendency for vertical motion to be suppressed: a fluid particle that does get displaced vertically tends to be restored to its original level; it may then overshoot inertially and oscillate about this level.
In this section we shall be examining the consequences of this in the simplest possible context: the internal waves. To study internal waves in their purest form, a few assumptions are necessary:

- there is no ambient rotation,
- the domain is infinite in all directions,
- there is no dissipative mechanism of any kind,
- the fluid motions and wave amplitudes are small.

This last assumption is made to permit the linearization of the governing equations. However, we reinstate a term previously neglected, namely, the vertical acceleration term $\partial w/\partial t$ in the vertical momentum equation. We do so anticipating that vertical accelerations may play an important role in gravity waves. The inclusion of this term breaks the hydrostatic balance. Finally, we decompose the fluid density as follows

$$\rho = \rho_0 + \bar{\rho}(z) + \rho'(z, t, z, t)$$

where ρ_0 is the reference density (a pure constant). $\bar{\rho}(z)$ is the ambient equilibrium stratification, and $\rho'(x, y, z, t)$ is the density fluctuation induced by the wave (lifting and lowering of the ambient stratification). The inequality $|\bar{\rho}| << \rho_0$ is enforced to justify the Boussinesq approximation, whereas the further inequality $|\rho'| << |\bar{\rho}|$ is required to linearize the wave problem.

The total pressure field is decomposed in a similar manner. With the preceding assumptions, the governing equations become

$$\frac{\partial u}{\partial t} = -\frac{1}{\rho_0}\frac{\partial \rho'}{\partial x} \tag{4.10}$$

$$\frac{\partial v}{\partial t} = -\frac{1}{\rho_0}\frac{\partial \rho'}{\partial y} \tag{4.11}$$

$$\frac{\partial w}{\partial t} = -\frac{1}{\rho_0}\frac{\partial \rho'}{\partial z} - \frac{1}{\rho_0} g\rho' \tag{4.12}$$

$$\frac{\partial u}{\partial x} + \frac{\partial v}{\partial y} + \frac{\partial w}{\partial z} = 0 \tag{4.13}$$

$$\frac{\partial \rho'}{\partial t} + w\frac{d\bar{\rho}}{dz} = 0 \tag{4.14}$$

$$\tag{4.15}$$

The factor $d\bar{\rho}/dz$ in the last term can be transformed by introducing the stratification frequency defined earlier. For simplicity, we will assume it to be uniform over the extent of the fluid. This corresponds to a linear density variation in the vertical. Because all coefficients in the preceding linear equations are constant, a wave solution of the form

$$e^{i(k_x x + k_y y + k_z z - \omega t)}$$

is sought. Transformation of the derivatives into products (e.g., $\partial/\partial x$ becomes ik_x) leads to a 5-by-5 homogeneous algebraic problem. The solution is non-zero if the determinant vanishes, and this requires that the wave frequency ω be given by

$$\omega^2 = N^2 \frac{k_x^2 + k_y^2}{k_x^2 + k_y^2 + k_z^2} \tag{4.16}$$

in terms of the wavenumber, k_x, k_y and k_z, and the stratification frequency, N. This is the dispersion relation of internal gravity waves.

A number of wave properties can be stated by examination of this relation. First and foremost, it is obvious that the numerator is always smaller than the denominator, meaning the wave frequency will never exceed the stratification frequency; that is

$$\omega \leq N$$

for positive frequencies. The reason for this upper bound can be traced back to the presence of the vertical acceleration term. Indeed, without that term the denominator in reduces from $k_x^2 + k_y^2 + k_z^2$ to only k_z^2, implying that the non-hydrostatic term may be neglected as long as $k_z^2 + k_y^2 < k_z^2$. This occurs

for waves with horizontal wavelengths much longer than their vertical wavelengths; the frequency of those waves is much less than N.
For progressively shorter waves, the correction becomes increasingly important, the frequency rises but saturates at the value N. We may then ask what would happen if we agitate a stratified fluid at a frequency greater than its own stratification frequency. The answer is that, with such short periods, fluid particles do not have the time to oscillate at their natural frequency and instead follow whatever displacements are forced upon them; the disturbance turns into a local patch of turbulence, and no energy is carried away by waves. Using a neutrally buoyant float in the ocean, D'Asaro and Lien (2000) have shown that in stratified waters values of ω/N in the range 0.2–1 generally correspond to internal waves whereas, at the same places, values above one ($1 < \omega/N < 50$) correspond to turbulent fluctuations.
Another important property derived from the dispersion relation 4.16 is that the frequency does not depend on the wavenumber magnitude (and thus on the wavelength) but only on its angle with respect to the horizontal plane. Indeed, with $k_x = k\cos\vartheta\cos\varphi$, $k_y = k\cos\vartheta\sin\varphi$, and $k_z = k\sin\vartheta$, where $k = (k_x^2 + k_y^2 + k_z^2)1/2$ is the wavenumber magnitude, ϑ is its angle from the horizontal (positive or negative), and ψ is the angle of its horizontal projection with the x–axis, we obtain

$$\omega = \pm N\cos\vartheta$$

proving that the frequency depends only on the pitch of the wavenumber, and, of course, the stratification frequency. The fact that two signs are allowed indicates that the wave can travel in one of two directions, upward or downward along the wavenumber direction. On the other hand, if the frequency is imposed (e.g., by tidal forcing), all waves regardless of wavelength propagate at fixed angles from the horizontal. The lower the frequency, the steeper the direction. At the limit of very low frequencies, the phase propagation is purely vertical ($\vartheta = 90°$).

Let us rotate the x and y axes so that the wavenumber vector is contained in the (x, z) vertical plane (i.e., $k_y = 0$ and there is no variation in the y-direction and no v velocity component).
The expressions for the remaining two velocity components and the density fluctuation are

$$u = -A\frac{g\omega k_z}{N^2 k_x}\sin(k_x x + k_z z - \omega t) \tag{4.17}$$

$$w = +A\frac{g\omega}{N^2}\sin(k_x x + k_z z - \omega t) \tag{4.18}$$

$$\tag{4.19}$$

$$p' = -A\frac{\rho_0 g k_z}{k_x^2 + k_z^2}\sin(k_x x + k_z z - \omega t) \tag{4.20}$$

$$\rho' = +A\rho_0 \cos(k_x x + k_z z - \omega t) \tag{4.21}$$

For k_x, k_z, and ω all positive, the structure of the wave is depicted on Figure 4.1.

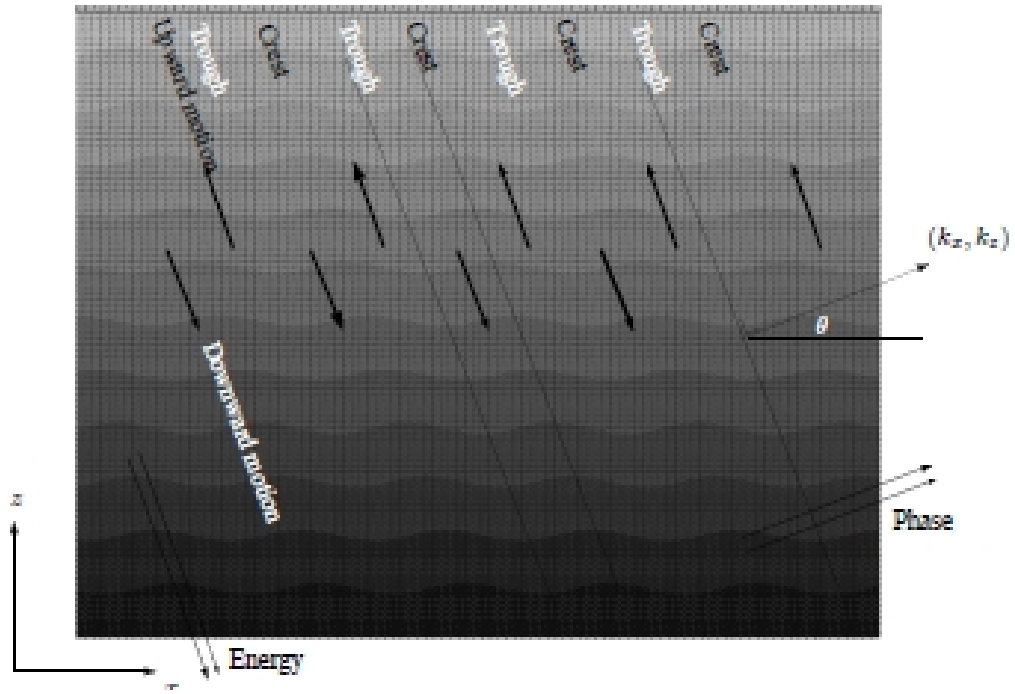

Figure 4.1: Vertical structure of an internal wave

The areas of upwelling (crests) and downwelling (troughs) alternate both horizontally and vertically, and lines of constant phase (e.g., following crests) tilt perpendicularly to the wavenumber vector. The trigonometric functions in the solution tell us that the phase $k_x x + k_z z - \omega t$ remains constant with time if one translates in the direction (k_x, k_z) of the wavenumber at the speed

$$c = \frac{\omega}{\sqrt{k_x^2 + k_z^2}}$$

This is the phase speed, at which lines of crests and troughs translate.
Because the velocity components, u and w, are in quadrature with the density fluctuations, the velocity is nil at the crests and troughs but is maximum a quarter of a wavelength away. The signs indicate that when one component is positive, the other is negative, implying downwelling to the right and

upwelling to the left, as indicated in Figure 4.1.
The ratio of velocities $(-k_x/k_z)$ further indicates that the flow is everywhere perpendicular to the wavenumber vector and thus parallel to the lines connecting crests and troughs. Internal waves are transverse waves.
A comparison of the signs in the expressions of w and ρ' reveals that rising motions occur ahead of crests and sinking motions occur ahead of troughs, eventually forming the next crests and troughs, respectively. Thus, the wave moves forward and, because of the inclination of its wavenumber, also upward.
The propagation of the energy is given by the group velocity, which is the gradient of the frequency with respect to the wavenumber

$$c_{gx} = \frac{\partial \omega}{\partial x} = +\frac{\omega k_z^2}{k_x(k_x^2 + k_z^2)} \tag{4.22}$$

$$c_{gz} = \frac{\partial \omega}{\partial z} = -\frac{\omega k_z}{k_x^2 + k_z^2} \tag{4.23}$$

$$\tag{4.24}$$

The direction is perpendicular to the wavenumber (k_x, k_z) and is downward. Thus, although crests and troughs appear to move upward, the energy actually sinks. It is possible verify that, irrespective of the signs of the frequency and wavenumber components, the phase and energy always propagate in the same horizontal direction (though not at the same rates) and in opposite vertical directions.

Let us now turn our attention to the extreme cases. The first one is that of a purely horizontal wavenumber $(k_z = 0, \vartheta = 0)$. The frequency is then N, and the phase speed is N/k_x. The absence of wavelike behavior in the vertical direction implies that all crests and troughs are vertically aligned. The motion is strictly vertical, and the group velocity vanishes, implying that the energy does not travel.
The opposite extreme is that of a purely vertical wavenumber $(k_x = 0, \vartheta = 90°)$. The frequency vanishes, implying a steady state. There is then no wave propagation. The velocity is purely horizontal and, of course, laterally uniform. The picture is that of a stack of horizontal sheets each moving, without distortion, with its own speed and in its own direction.
If a boundary obstructs the flow at some depth, none of the fluid at that depth, however remote from the obstacle, is allowed to move. This phenomenon, occurring at very low frequencies in highly stratified fluids.

Chapter 5

Numerical experiment B

Starting by the numerical experiment presented in chapter 3, we want now see what happens by adding the stratification effects. The results obtained in this way can be considered as the vertical section of a three-dimensional stratified flow.
To have a situation as close as possible to that of departure, we created an initial density field by combining two constant density field with the same hyperbolic tangent used for the vorticity field. In particular, we divided the density field as follows:

$$\rho = \rho_0 + \bar{\rho}(y) + \rho'(x, y, t)$$

where ρ_0 is a constant, $\bar{\rho}(y)$ is a linear function and ρ' is the fluctuation component. The trend of this components are shown in figure 5.1

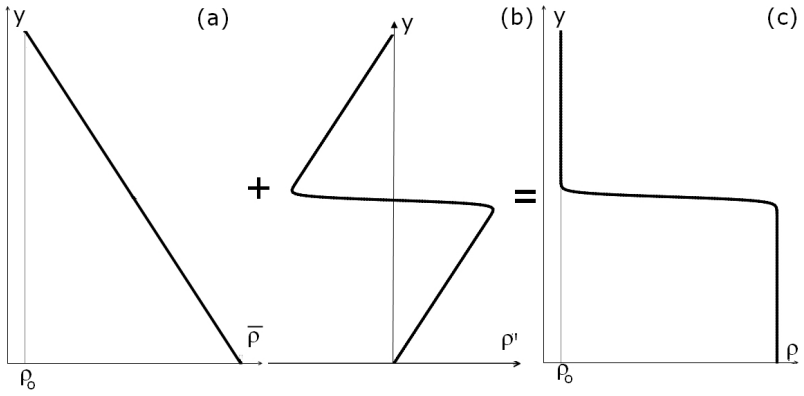

Figure 5.1: Initial density fields: (a) is the linear function, (b) fluctuation part, (c) total density

In this contest, using the Boussinesq approximation, the equation that we are going to resolve are the follows

$$\begin{cases} \nabla \cdot \mathbf{u} = 0 \\ \dfrac{\partial \mathbf{u}}{\partial t} + (\mathbf{u} \cdot \nabla)\mathbf{u} = -\dfrac{1}{\rho_0}\nabla p - \dfrac{\rho'}{\rho_0} g\hat{j} + \nu \nabla^4 \mathbf{u} \\ \dfrac{\partial \rho'}{\partial t} + \mathbf{u} \cdot \nabla \rho' + v\dfrac{d\bar{\rho}}{dy} = k\nabla^2 \rho' \end{cases}$$

The last equation is a model equation to close the problem. As we said in the previous chapter, density variation in the vertical direction are generally caused by variation of temperature and concentration (for example, variation of salinity in the oceanic flows).
If we had not used this model, our system (and code) would have been considerably more complicated because we should have added a transport-diffusion equation for each variable that influences density along the equations that link these entities to density.
On the contrary, we have gathered all these effects in our third equation and, using more lab tests (as the ones made by Waraft [17]), it is possible to better estimate all the coefficients, according to what we are aiming to simulate.
In this way, we can explain the presence of the diffusive term in a density equation, even if this term would have no meaning from a strictly physics point of view. k, the diffusion coefficient for this variable and in our simulation is always equal to $0.3\ 10^{-2}\,[m^2/s]$. We can also define a pseudo Schmidt number as $Sc = \frac{\nu}{k^2} = 1.32\ 10^{-4}$

Note that we can still use periodic boundary condition because ρ' is periodic and $\bar{\rho}$ appears only as a derivatives and thus as a constant.

In the present study, we have fixed the energy ratio at 6.6 and the Froude number has been chosen as the sole control parameter. In particular we have compared the results obtained in the case without stratification with the stratified flow at Froude number equal to 10 and 0.1 The other parameter of the simulation are the same that introduced in chapter 3. Also the data analysis will be carried out following, as far as possible, the same pattern used for the previous numerical experiment.

5.1 Numerical method

To obtain these new simulations it was, obviously, necessary modify the code. First of all we have chose as inhomogeneous direction the gravity direction, i.e. y, in other word we have rotate our vorticity field.
Then the variables of the density field were added at the code and we have

wrote a function to create the initial fluctuating density field. This function operates as follows:

- read the density gradient, α, which must be negative for a stable stratification,
- create the total density field with this operation

$$p(y) = \frac{1}{2}\left[1 + \tanh\left(a\frac{y}{L}\right)\tanh\left(a\frac{y - L/2}{L}\right)\tanh\left(a\frac{y-L}{L}\right)\right]$$

$$\rho(\cdot, y) = \rho_1 p(y) + \rho_2\left[1 - p(y)\right]$$

  where $\rho_1 = -\alpha 2\pi$ and $\rho_2 = 0$
- change the value of ρ in the vertical extremes of the domain in order to satisfy the periodicity condition. In this way we obtain the function shown in figure 5.1(c)
- subtract the linear function $\bar{\rho} = \alpha y + \rho_1$ and yields the fluctuating density fields shown in 5.1(b).

Then we have wrote the subroutines for time evolution of ρ'. In so doing, we used the same logic with which the vorticity was resolved previously. In the spectral space, the equation to solve is:

$$\frac{d}{dt}\left(\underbrace{e^{-kk^2t}\hat{\omega}}_{\hat{r}}\right) = \underbrace{\left(-\hat{J} - \frac{ik_x}{k^2}\alpha\hat{\omega}\right)}_{\hat{nlt}} e^{-\nu k^2 t} \qquad \Rightarrow \qquad \frac{d}{dt}\hat{r} = -\hat{nlt}e^{-\nu k^2 t}$$

To calculate the non linear term, first we evaluate the velocity $(u, -v)$ from the vorticity in the spectral space in this way

$$\hat{u} = -\frac{ik_y}{k^2}\hat{\omega} \qquad \hat{v} = \frac{ik_x}{k^2}\hat{\omega}$$

Then we call the FFT inverse to return in the physical space and so we can calculate the products $r_1 = \rho'\omega$ and $r_2 = \rho'\omega$. Then we can call the FFT for r_1 and r_2 and finally we can compute the non linear term as follows

$$\hat{nlt}_\rho = ik_x\hat{p}_2 - ik_y \underbrace{-\frac{ik_x}{k^2}\alpha}_{grad(k_x,k_y)} \hat{\omega}\hat{p}_1 \tag{5.1}$$

where the term $grad(k_x, k_y)$ is calculated solely in the function that define the spectral vector. To conclude, we have also changed the vorticity non linear term, defined in 3.2, adding the gravity term as follows:

$$\hat{nlt}_\omega = ik_x\hat{p}_2 - ik_y\hat{p}_1 - ik_x\frac{g}{\rho_0}\hat{\rho}' \tag{5.2}$$

5.2 Simulation results and discussion

The initial conditions place a kinetic energy gradient in the direction of the gravity. As seen in the previous chapter, the stratification tends to inhibit vertical motions. At the same time, however, the previous numerical experiment shows the existence of a turbulent diffusion velocity in the inhomogeneity direction. We must therefore understand which of the two effects prevails. Is intuitive to suppose that this depends on the Froude number.

To better understand what happens we're going to see some graphic results.

In the figure 5.2 we show the time evolution of density and vorticity with Fr = 10, i.e. in a flow is not strongly stratified. Regarding the density field, there was a significant interaction between the two initial fields. This is due mostly to the term $v\alpha$ and suggests that the rate of turbulent diffusion is still dominant in relation to gravity. This is confirmed by the vorticity where we can still see the completion of mixing between the two initial fields.

In figure 5.3 we have the similar results for Fr = 0.1, i.e. by increasing the stratification of a factor thousand. This change leads to significant changes in the pattern of the flow. The two density fields can not interact and seem almost frozen in the initial conditions. Only the thickness of the mixing layer increases slightly over time. Furthermore, inhibition of vertical motion is prevalent enough to lead to a layer of zero vorticity in the middle of the domain. This is a typical internal wave characteristics of the stratified flows. Importantly, this is not due to the fact that the turbulent diffusion go up and gravity down but only to the inhibition of vertical motions: if we inverted the initial vorticity field we would have the same situation but reversed. We then found the first key result of these simulations: the penetration occurs only for large enough Froude numbers. Find the level of stratification that discriminates the two behaviors could be future studies on this type of problem.

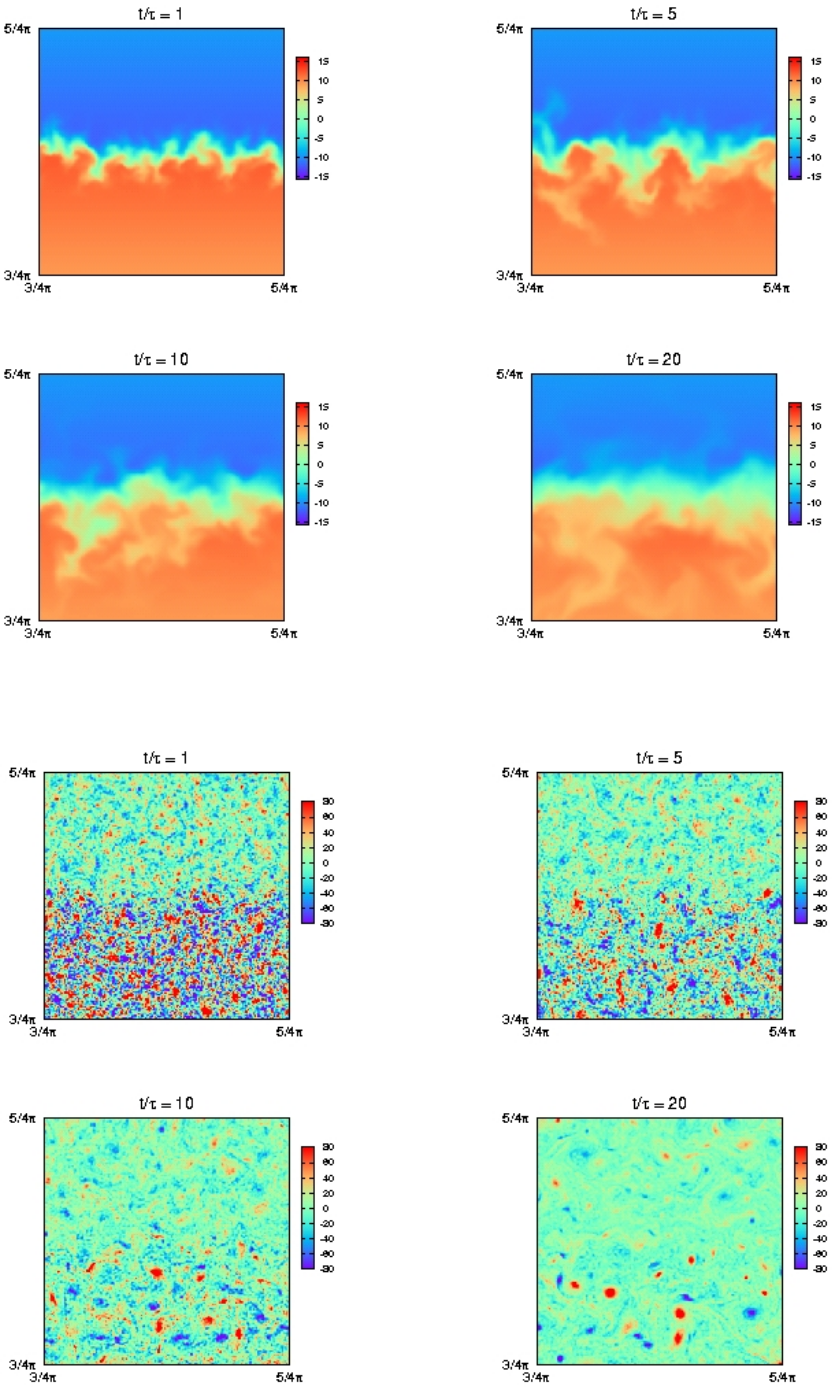

Figure 5.2: Visualization at four time instants of density (top) and vorticity (bottom) contours, which Fr=10, in the central zone of the analytical domain

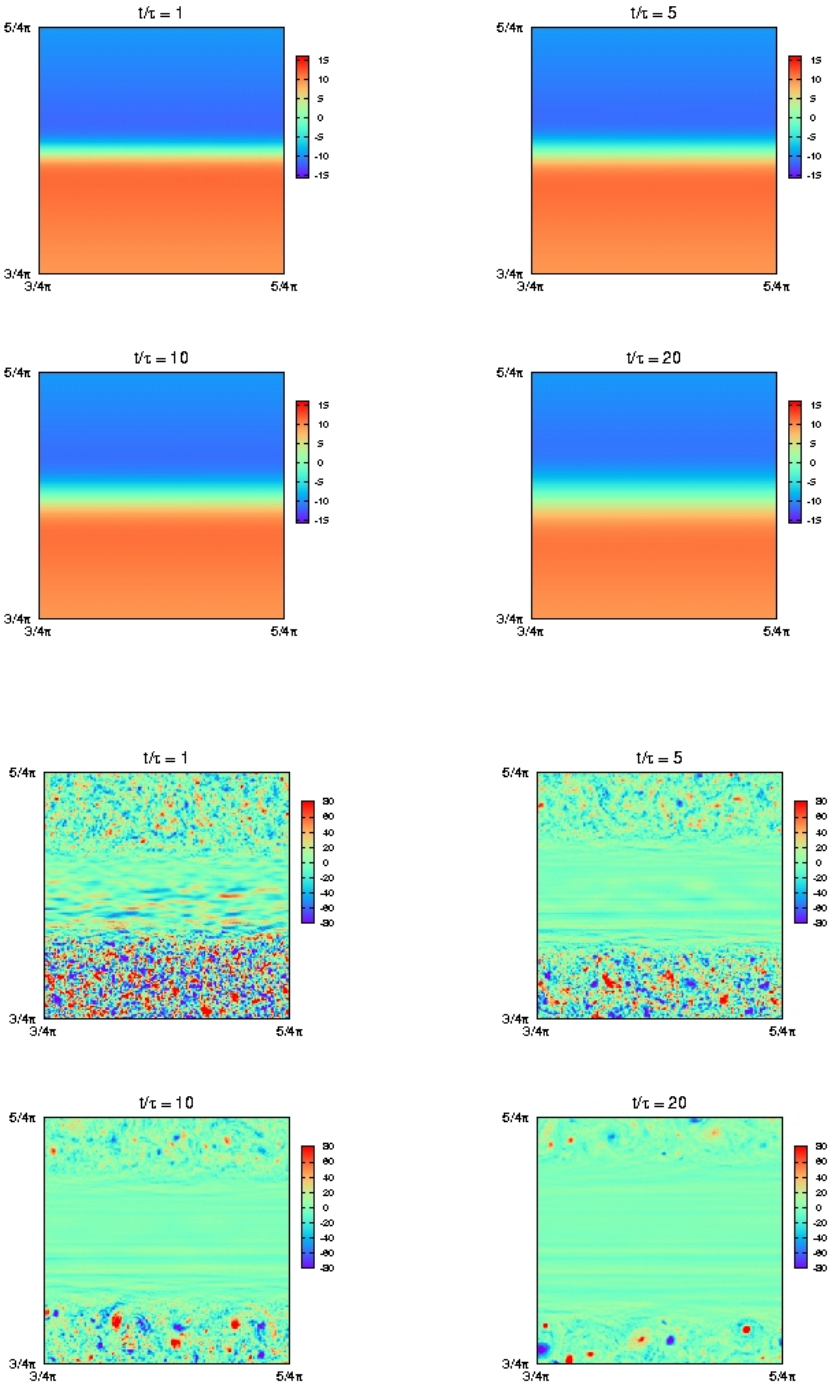

Figure 5.3: Visualization at four time instants of vorticity contours, which Fr=0.1, in the central zone of the analytical domain

Analysis of the results continues in the next section where we estimate the length scale evolution in the different cases. To do this we will analyze the kinetic energy and the total density profile. In section 5.2.2 we do statistics analyses on velocity moments to see the intermittent behavior of the flow.
Adding the forcing term, the long-range interactions between fluid particles are hidden by the force of gravity, and then study the autocorrelations in time of vorticity is meaningless.

5.2.1 Qualitative Universality

As mentioned in section 4.4, stratified flows can support a variety of types of wave motion, which have no counterparts in unstratified fluids since the tendency for vertical motion to be suppressed.
In the previous section we have anticipated what this means in our case. Now let us to make a more detailed analysis that will lead us to estimate as the mixing layer thickness varies as a function of Froude number.
To do so is very useful to examine the profile of kinetic energy in various cases as is shown in figure 5.2.1.

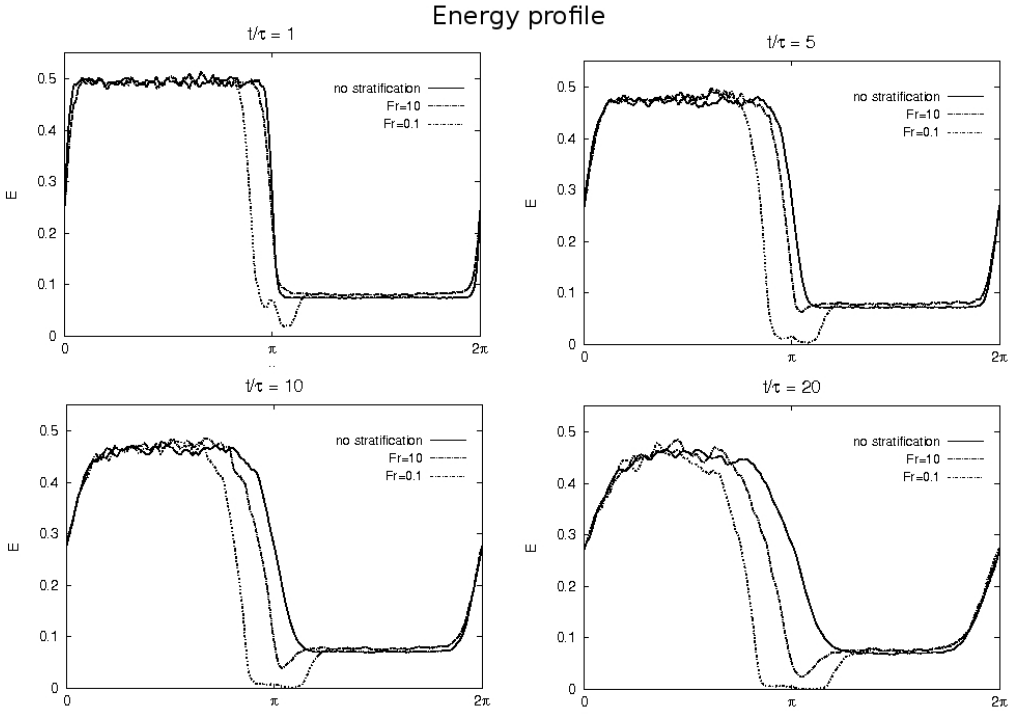

Figure 5.4: Time evolution of the energy profile with different Fr

First we observed a sharp decrease of energy in the mixing interface. This is reasonable since this is the only area in which a density gradient is present from initial time. So close to interface the work done by buoyancy forces reaches its maximum value and the interface behaves like a energy well.
At the edge of the domain instead we have developed independent of the Froude number. This is because the density is constant at the boundary. It is clear that in this situation is no longer possible do the same type of analysis of the unstratified case. It has not sense to speak of penetration and also the definition of Δ given previously here becomes meaningless because the energy is no longer a monotonous pattern.
But we can still define the mixing layer basing on the total density profile as the distance between the points with a density value equal to 25% and 75% of maximum density.
Figure 5.5 shows the time evolution of the total density profile in the three cases considered, while in figure 5.6 is represented the evolution of mixing layers corresponding.

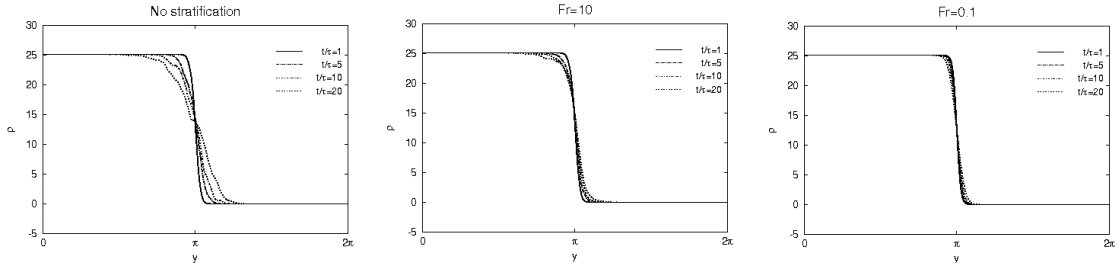

Figure 5.5: Time evolution of the total density profile in the different intensity of stratification considered

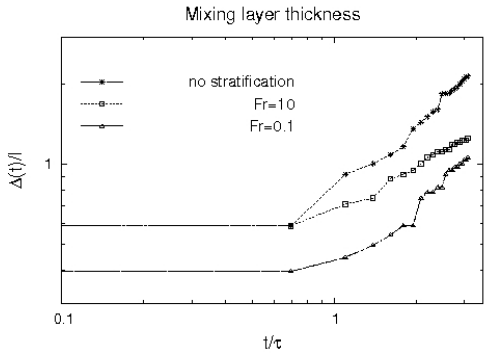

Figure 5.6: Mixing layer thickness as a function of the normalized time with different Fr

The final thickness of the layer of mixing decreases with increasing stratification. By executing a best fit, we can estimate the asymptotic behavior with the follows slope:

- No stratification → 0.7226
- Fr=10 → 0.302
- Fr=0.1 → 0.2818

Clearly we have not yet enough data to make a reasonable fit of these results.

5.2.2 Large- and Small- Scale coherent structures

In this section we analyze the skewness and the kurtosis distribution of the velocity in order to see the intermittent behavior of the flow. In the not stratified case, we saw that the intermittent behavior was mostly concentrated in the area of mixing. For Froude numbers less than infinity intermittence extends even beyond. Look at the trend of skewness shown in figure 5.7

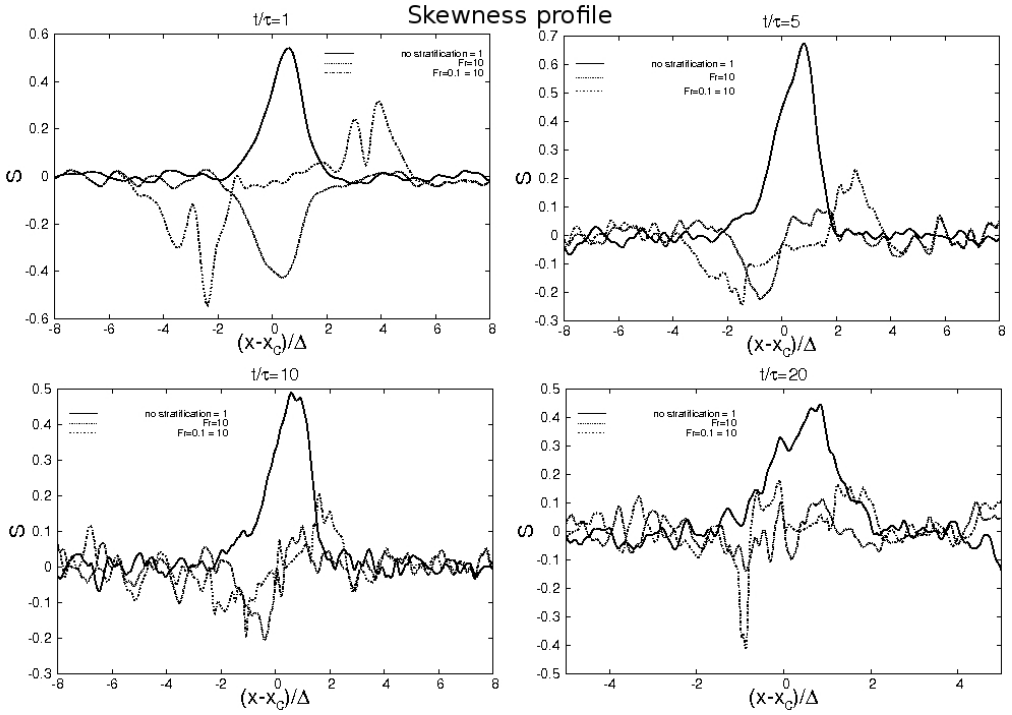

Figure 5.7: Skewness of the velocity component in the inhomogeneous direction for each Fr. x_c is the mixing layer center and Δ is the mixing layer thickness

For stratification very intense, at the initial time the skewness presents almost a symmetry: in the high energy the skewness is negative, in the low energy is positive and is zero in the separation layer. This trend is preserved in time but the peaks become lower and central area shrinks. In the last moments the skewness zero zone disappears and a peak is predominant at the interface between zones of high energy and layer separation.

Conversely, the intermediate case initially presents a nearly symmetrical distribution of the third moments when compared to the unstratified case. Evolving over time the peak moves increasingly moving to the left. It is important to note that the position of the maximum skewness shifts to the left. This means that despite the vorticity fields continue to interact with each other, the penetration as defined in 3.2.1 is negative. In other words, even for Froude numbers greater than one, inhibition of vertical motion generates an inverse penetration.

The intermittent flow may also be analyzed by looking at the fourth moment of v.It is shown in figure 5.8

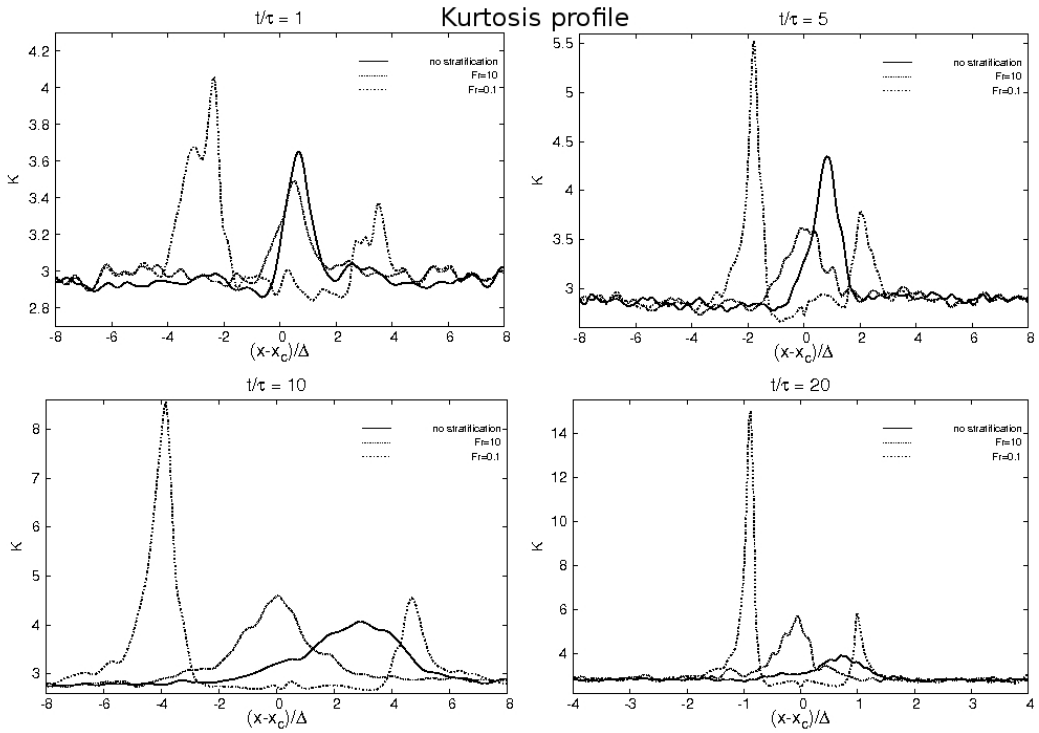

Figure 5.8: Kurtosis of the velocity component in the inhomogeneous direction for each Fr. x_c is the mixing layer center and Δ is the mixing layer thickness

Similar to before, for Fr = 0.1 there are two peaks: one at the interface between zones of high energy and the middle layer and a smaller one at the other interface. These peaks are getting higher and more distant in the evolution of time. For Fr = 10 we have not evolved very far from what occurs in the non stratified case, but the peak is slightly lower and moving to the left, i.e. towards the area of high energy.

Chapter 6

Conclusion

We first considered the simplest kind of two dimensional turbulent shearless mixing process which is due to the interaction of two isotropic turbulent field with different kinetic energy but the same spectrum shape. This mixing is characterized by the absence of advection, production of turbulent kinetic energy, and an integral scale gradient. First, we demonstrated that, in this situation, asymptotically in time, the turbulent diffusion is infinitely greater than that measured in three dimensions.
We then analyzed the third and fourth moments of velocity. This analysis indicates that the flow is highly intermittent. This refutes the thinking of many who believe that the departure from Gaussianity is impossible in 2D turbulence which is absent in the phenomenon of vortex stretching.
Finally we estimated the time in which the solution "forgets" the initial condition by studying the autocorrelation time of the vorticity at different points. We discovered that this does not depend neither by the points selected, neither by the ratio of energy used. The vorticity is almost completely unrelated after 5 LETOT but retains a dependence of 3% even after 20 time units. The autocorrelation function is proportional to $t^{-0.8}$ and this indicates the presence of a long-range interaction.

Later we changed the experiment by adding the effect of a stable stratification. This changes significantly the evolution of the flow.
First, we have observed for small Froude numbers the two fields can not interact through the central area of domains, where it forms a layer of zero-vorticity separation. Under this layer forms a energy well. The reason is because some kinetic energy is being converted into potential energy by the gravity force. By skewness analysis, we see that there is a inverse penetration even for stratification not too strong. Finally, defining the thickness of mixing on the total density profile, we have seen that its asymptotic behavior is exponential with a slope that decreases with decreasing of Fr.

Bibliography

[1] C. Canuto, M.Y. Hussaini, A. Quarteroni, and T.A. Zang. *Spectral method. Fundamentals in single domains*. Springerl, 2006.

[2] P.A. Davidson. *An introduction to magnetohydrodynamics*. Cambridge university press, 1988.

[3] U. Frish. *Turbulence: The legacy of A.N.Kolmogorov*. Cambidge University Press, 1995.

[4] U. Frish and G. Parisi. A multifractal model of intermittency. in turbulence and predictability in geophisical fluid dynamics and climate dynamics. 1985.

[5] J. Hinze. *Turbulence*. McGraw-Hill, 1959.

[6] H. Kellay and W. Goldburg. Two-dimensional turbulence: a review of some recent experiment. *Rep. Prog. Phys.*, 65, 2002.

[7] A. Kolmogorov. The local structure of turbulence in incompressible viscous fluid flow for very large reynolds number. *Dokl. Akad. Nauk*, 26, 1941.

[8] A. Kolmogorov. A refinement of previous hypotesis concerning the local structure of turbulence in incompressible viscous fluid at high reynolds number. *J. Fluid Mech*, 13, 1962.

[9] P. Kundu and I. Cohen. *Fluid Mechanics*. Academic press, 2002.

[10] L. Landau and E. Lifshitz. *Fluid mechanics 2nd ed.* 1987.

[11] L. Richardson. *Weather prediction by numerical process*. Cambidge University Press, 1992.

[12] J. Riley and S.M. deBruynKops. Dynamics of turbulence strongly influenced by buoyancy. *Phys. Fluids*, 15, 2003.

[13] J. Riley and M.P. Lelong. Fluid motions in the presence of strong stable stratification. *Ann. Rev. Fluid Mech.*, 32, 2000.

[14] D. Tordella and M. Iovieno. Numerical experiments on the intermediate asymptotics of shear-free turbulent transport and diffusion. *J.Fluid Mech.*, 549, 2006.

[15] D. Tordella, M. Iovieno, and P.R. Bailey. Sufficient condition for gaussian departure in turbulence. *Phys.Rev.*, 77, 2008.

[16] D.J. Tritton. *Physical fluid dynamics*. Oxford science publications, 2006.

[17] S. Veeravalli and Z. Warhaft. The shearless turbulence mixing layer. *J. Fluid. Mech.*, 207, 1989.

List of Figures